Influence of Flow Disruptors on the Performance of Piezoelectric Cantilever Beams for Energy Harvesting Through CFD Analysis

a project presented to
The Faculty of the Department of Aerospace Engineering
San José State University

in partial fulfillment of the requirements for the degree
Master of Science in Aerospace Engineering

by

Andrew D. Gasser

May 2025

approved by

Dr. Edoardo Rubino
Faculty Advisor

Abstract

Influence of Flow Disruptors on the Performance of Piezoelectric Cantilever Beams for Energy Harvesting Through CFD Analysis

Andrew D. Gasser

Piezoelectric materials provide a unique solution to harvest energy due to their capability of creating a power output when subjected to an external load and therefore to an internal strain. Utilizing turbulence from fluid flow to harvest energy is a relatively under-researched field, leaving the potential for more efficient and easier to maintain energy harvesting systems. This project aims to study energy harvesting devices based on flow disruptors and piezoelectric cantilever beams. In particular, the goal is to understand how the turbulence created by the flow disruptor can be used to improve the performances of the piezoelectric beams, and to investigate the effect of several parameters such as the dimensions of the components and their relative position. Multiple geometric configurations were simulated in COMSOL FSI to determine what conditions yielded the highest power output. It was determined that certain configurations yielded desirable piezoelectric beam behavior that produced constant energy output in steady state conditions. The potential for higher power output at a larger scale is promising, as only a single harvester at low velocity was simulated.

Acknowledgment

I would like to thank my advisor, Dr. Edoardo Rubino, for his expertise and guidance throughout this entire project. I would also like to thank Dr. Yawo Ezunkpe, for providing further guidance in the details of fluid dynamics. Lastly, I would like to thank my family, whose support allowed me to both complete this project and pursue what I am truly passionate about.

Table of Contents

List of Figures

List of Tables

Symbols

Symbol	Definition	Units
$\vec{u}_f$	Velocity vector	m/s
P	Pressure	Pa
u	Horizontal flow	m/s
F	Deformation gradient tensor	-------
S	Stress tensor	-------
f_v	Body forces	N
I	Identity matrix	-------
D	Electric displacement	C/m^2
S	Strain	-------
T	Stress	Pa
E	Electric field intensity	N/C
s	Elastic compliance	TPa
d	Piezoelectric coefficient	-------
Greek Symbols		
ρ	Density	kg/m^3
μ	Fluid viscosity	Pa * s
$\vec{u}_{solid}$	Displacement field	C/m^2
ε	Permittivity	F/m
Subscripts		
$( )_f$	Fluid property	-------
$( )_s$	Solid property	-------
$( )_v$	Piezoelectric property	-------

Acronyms		
CFD	Computational Fluid Dynamics	-------
FSI	Fluid Structure Interaction	-------
PZT	Lead Zirconate Titanate	-------
FEA	Finite Element Analysis	-------
PVDF	Polyvinylidene Fluoride	-------
RANS	Reynolds-averaged Navier–Stokes	-------
VIPEC	Vortex-Induced Piezoelectric Energy Converter	-------

1. Introduction & Literature Review

1.1. Motivation

Energy consumption of the United States of America is projected to increase anywhere from 0-15% in the next 25 years with no significant plan to fill these increased demands. Specifically in the industrial sector, as much as a 32% increase in energy consumption is projected [1]. The growing demand for energy without a plan for where the energy will be provided has been a persistent problem in the talks of the global energy crisis, with the need to address this demand with renewable energy sources. The most popular forms of renewable energy today include solar and wind energy, but these factors are limited by weather, geography, and the need for maintenance [2]. Due to these variables, piezoelectric materials offer a solution, as the strategic placement and utilization of these materials will allow for round-the-clock energy production with minimal maintenance. These materials offer the unique opportunity to harvest energy from both natural and unnatural sources of vibration and turbulence in the environment they exist in.

Currently, piezoelectric materials are mostly used in modern-day electronics, such as televisions, watches, and automobiles [3]. There has also been research and prototypes of using the technology in areas of everyday life. Companies like Pavegen have created piezoelectric tiles that generate electricity as humans walk over them. While this idea is creative, the overall energy output is dependent on the human traffic in a given sector. The goal of this research is to provide insight into the potential use of piezoelectric materials in energy harvesting, particularly in the harvesting of energy from turbulent fluid flow. Specifically, this literature review will first examine both the past and present of piezoelectric materials, then energy harvesting using piezoelectric materials, and lastly the use of fluids and CFD in harvesting energy through piezoelectric materials.

1.2. Literature review

The scope of this literature review is to investigate the current literature surrounding piezoelectric materials and the research utilizing them in energy harvesting. Particularly, there will be an investigation in the use of piezoelectric materials and their use in harvesting energy from turbulent flow. This information will be essential to the development of research towards the optimization of fluid flow disruptors in energy harvesting configurations. This literature review will first look at the history of piezoelectric materials, then into modern piezoelectric materials, then energy harvesting with piezoelectric materials, and finally fluid flow harvesting with CFD to back up the research.

1.2.1. History

The direct piezoelectric effect was first discovered in 1880 by the Curie brothers, Pierre and Jacques [4]. Their research was primarily focused on quartz crystals and their behavior under mechanical stress. In the next year, the converse piezoelectric effect, a phenomenon that describes geometric strain in relation to an electric field applied to piezoelectric materials, was discovered by Gabriel Lippmann. The first major technological breakthroughs occurred in the early 1900s, during World War I in the use of ultrasonic technology to search for U-boats. This

ultrasonic technology ended up becoming sonar, which was constructed by placing piezoelectric material between two steel plates and creating high-frequency vibrations, and a hydrophone to detect the vibrations coming back [5]. This sonar device utilizes a similar structure that is seen in current day piezoelectric materials, laying the ground work for future innovations in the field. From that point on, the material gained the interest of many industries and was integrated into different technologies.

1.2.2. Modern Piezoelectric Materials

Piezoelectric materials have developed significantly from the 1800s when they were first discovered and experimented with. Current day piezoelectric materials are much more complex, as they comprise blends of many more materials than the basic single quartz or Rochelle salt crystal that was used in the past. Typically, piezoelectric materials can be categorized into five main groups: monocrystals, piezoelectric polycrystals (piezoelectric ceramics), polymers, semiconductors, and composites [6]. Monocrystals have very good performance and are stable, but they can be expensive and have a relatively low piezoelectric coefficient. These crystals include the quartz crystals that were experimented on when piezoelectricity was first discovered.

Ceramic blends have become one of the more popular blends used in piezoelectric materials, with titanate and niobate composites being used in most commercial energy harvesting components [7] [8]. They have a short response time and are highly sensitive but are brittle, have poor fatigue resistance, and have low bending deformation. The most common ceramic composite with the longest historical performance is lead zirconate titanate (PZT). This ceramic composite was the predecessor of single crystal piezoelectric materials, being much more reliable. Many energy harvesting components purchasable online contain PZT. One modern downside of PZT is the presence of lead in the ceramic material. Lead based ceramics have led to safety concerns while integrating piezoelectric materials into various technologies, such as biocompatibility in wearable devices. This has been the topic of some research in the attempts to synthetically create a lead-free ceramic piezoelectric material [9]. Should the results of this research prove possible, it would allow for wearer and environmentally safe ceramic piezoelectric materials to be more available. One of the major benefits of ceramic-based piezoelectric materials is the high strain constant, or its “d” coefficient. This value relates the output mechanical strain to the applied electrical field. This characteristic is most useful in devices that will produce a physical response to an electric current, such as electronic speakers. While this characteristic does not fit the ideal description for energy harvesting, ceramic based piezoelectric materials still possess the ability to produce energy from mechanical strain, but it is not as efficient as its inverse effect.

The third category of piezoelectric materials, polymers, are another common material used due to its flexibility and high voltage output, with the downside being a lower piezoelectric signal being generated and a limited temperature range [8] [10]. The important aspect of polymer piezoelectric materials in the scope of this research is the voltage constant, or the “g” coefficient. This value is the numerical constant that describes the voltage produced by mechanical stress, which for energy harvesting is the most important factor to consider.

Another form of piezoelectric materials is piezoelectric semiconductors. These materials posses the qualities of both semiconductors and piezoelectric materials, and act as unique solutions to certain problems. Some piezoelectric materials have semiconductor qualities, such as PZT being a p-type semiconductor [11].

The last category of piezoelectric materials are composites. These materials are a combination of an existing piezoelectric material and some other non-piezoelectric material. The goal of these blends is to enhance the performance of a material without compromising other properties. An example of these blends includes the combination of Macro Fiber Composites with PZT [12]. PZT by itself is a relatively brittle material, but by integrating more elastic fibers into the material and then analyzing it with FEA, the benefits of the composite could be been seen. Another example of composites that does not fit the typical definition can be seen in the research of Savin et al., where they and their team studied the effects of combining PZT into a polymer-based piezoelectric material, polyvinylidene fluoride (PVDF) [10]. By blending 10% PZT into the PDVF, the researchers were able to increase the piezoelectric response while keeping stress values within operational requirements. This type of composite would be extremely valuable as it would allow for a wider range of applications for piezoelectric materials in the scope of energy harvesting.

1.2.3. Devices and Applications for Energy Harvesting with Piezoelectric Materials

The principle of harvesting energy while using piezoelectric materials is based on harnessing the ambient or parasitic mechanical energy that exists in systems. This can be through more conventional means such as bladeless wind turbines or more creative means such as piezoelectric tiles in busy cities. Energy harvesting using piezoelectric materials can be broken down into one of two categories: harvesting energy from periodic compressive loads or harvesting energy from excess vibrations. Both of these categories will typically harvest energy with one of the four following, or through a combination of the four: cantilever beam, circular diaphragm. cymbal type, or stack type (Figures 1.1-1.4) [13].

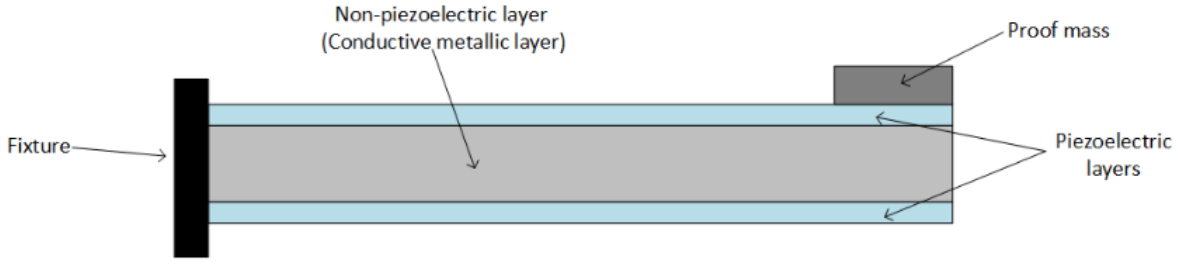

Figure 1.1 - Cantilever beam

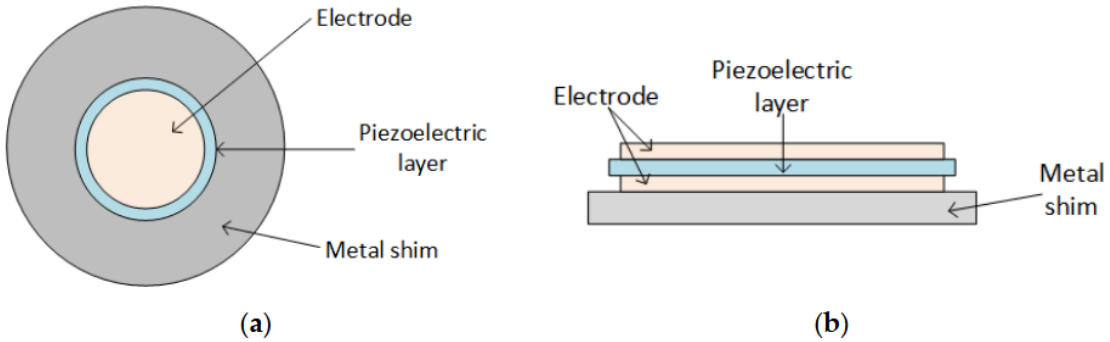

Figure 1.2 - Circular diaphragm

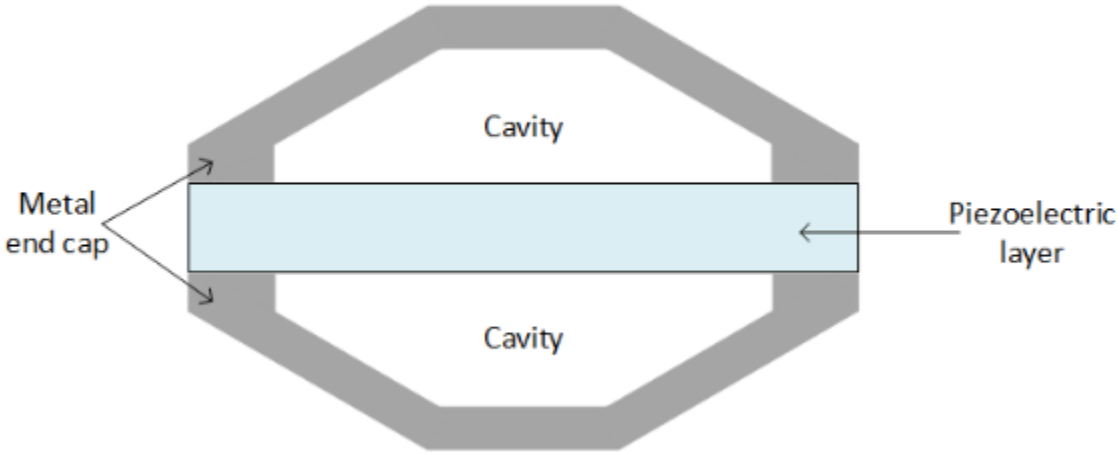

Figure 1.3 - Cymbal type

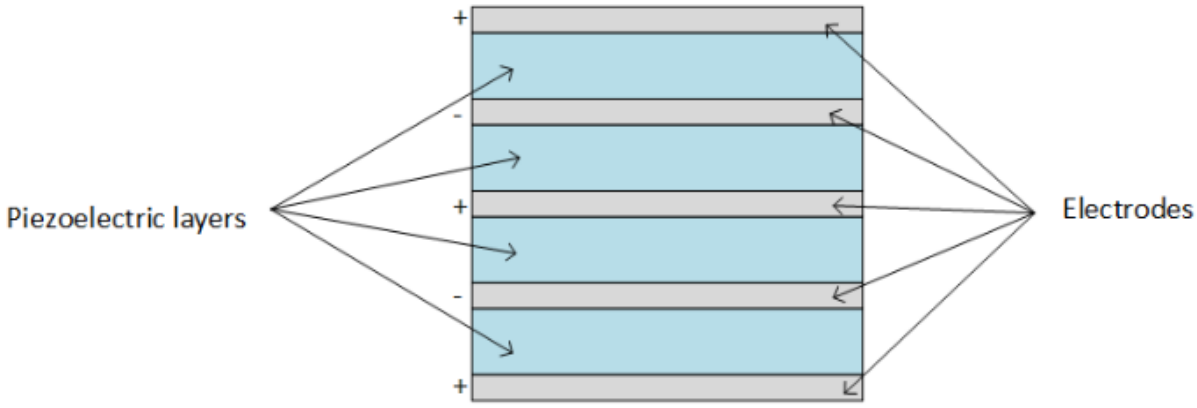

Figure 1.4 - Stack transducer

The cantilever beam harvester consists of one or two piezoelectric layers, surrounding a non-piezoelectric material that is conductive and gives structural support. Due to the fact that piezoelectric materials can be brittle, the structural material must provide enough support to prevent excess bending that would damage the material, while simultaneously being pliable enough for the beam to flex and generate an electric charge. This is the most simple design, leading to straightforward implementation and ease of manufacturing. These devices will be the energy harvesters that will be used in this research.

The circular diaphragm harvester contains a layer of piezoelectric material, with two electrodes on either side on top of some type of substrate. This design usually undergoes compressive loads, making it ideal for sensors [14]. However, the design can be modified to act as an energy harvester, ideally for vibrating compressive loads over a period of time.

The cymbal type harvesters consist of a layer of piezoelectric material between two metal plates. When the metal plates undergo compression, they stretch the piezoelectric material, generating a charge. One potential area of energy lost can be found in the metal plates deforming, where instead of all the energy being transferred to the piezoelectric material, it is

instead transferred to the metal [15]. This harvester is similar to the circular diaphragm type as they both deal with compressive loads, but the cymbal places the load in a different direction and can take higher loads of force due to the metal plates.

The stack transducer harvester makes use of multiple piezoelectric materials stacked on top of each other. Through this design, high mechanical loads are able to be withstood [13]. However, due to the nature of multiple piezoelectric materials being stacked on each other, the device has a relatively high stiffness, which could be used to the benefit of the device if it is utilized properly.

Being that cantilever beams are one of the easiest designs to work with, there are many applications for them. Heller et al. look at the integration of cantilever beams into the pavement of roads to harness the vibrations from passing vehicles [16]. Their study consists of boxes containing an array of cantilever beams that are integrated into the road where the vibrations of passing vehicles are then transferred to the piezoelectric material. The researchers concluded that their prototype was effective and was able to achieve the goal of their study, which was to power an electric sign nearby. While their study tested two different tip masses, a laboratory test with a variety of tip masses to test maximum voltage output versus durability would have been a preferable addition to the study. By taking the data collected from the road tests, the researchers could have then simulated the environment in a lab to determine optimal configurations. Other researchers from Bangkok, Tuma and Phaoharuhansa, ran an FEA analysis of a double-piezoelectric beam meant to harvest energy from low-frequency vibrations [17]. By using a double beam, the researchers were able to harness energy from multiple frequencies, therefore increasing the effective range of the piezoelectric beams. Should this configuration be implemented into other systems such as the pavement harvesting system mentioned above, it could increase the efficiency of the systems. The study from Tuma and Phaoharuhansa could have benefited from discussing potential applications of their study, taking their study from purely theoretical to practical applications. An example of fluid energy harvesting using cantilever beams can be found in the research of Yayla et al. [18]. Their research utilizes a turbulence generator in a fluid flow, for example, a river, to turn laminar flow turbulent. At the point of highest turbulence, a cantilever piezoelectric beam was placed to convert the turbulence into electrical energy. Two turbulence generators were investigated in the study, which were plates with holes that directed the water in specific directions to generate the highest levels of turbulence. Their research was verified with both CFD and experimental data, investigating both the different turbulence generators and the distance of the cantilever piezoelectric beam from the generators. By using multiple forms of data, their results were able to verify each other. While the study was very well structured, the potential applications are debatable. The principle of the study is based on having a large body of water funnel into a smaller subsection, essentially diverting the flow. Current energy harvesters that utilize water tend to work with the direction of water instead of diverting it, so in order for this to be implemented a significant amount of infrastructure would be necessary. These studies help illustrate the versatility of the piezoelectric cantilever beam in energy harvesting. In just a couple of studies, the range of applications for the cantilever beam was shown in both the area of research and physical systems.

While piezoelectric cantilever beams are the most popular form of energy harvesting, the other three devices mentioned above are still used in different forms of research. The circular diaphragm is most commonly used in sensors, but Chen et al. investigated the potential use of the design in energy harvesting [14]. This study consisted of a piezoelectric circular plate with a load placed on top in a vibrating system. The two variables that were investigated were loads up to

1.2 newtons and resistance, determining the optimal frequency for each configuration. This study brought to light the fact that certain configurations are limited to a small range of ideal frequencies for energy harvesting. Changing the resistance tended to do little to change the ideal frequency, while changing the load would shift the ideal frequency significantly. However, there are limitations to the range of the load, as a larger load tended to release more energy at a lower ideal frequency, and a small load released less energy at a higher frequency. This study shows that this configuration would only be ideal for harvesting energy at lower frequencies and higher loads, so using it in a high-frequency environment would be counterproductive, regardless of the changes in load or resistance.

Another application of piezoelectric energy harvesters has been seen in integrating the material in wearable clothes. Palosaari et al. researched the integration of cymbal type harvesters in the heel of shoes in their study [15]. By placing the harvester in the shoe, it takes advantage of the constant steps of humans and the compression of their steps to generate electricity. The integration of this technology could serve multiple purposes, by replicating and replacing the absorbent material in the heel of the shoe, not taking up any unnecessary space. In their study, they observe a range of steel plate thicknesses at a range of forces from 0 to 35 Newtons. Realistically, only small children fall into that category of weight, meaning the applications of their technology only applies at small scales such as powering light up sneakers. They then go on to explain that this technology could be implemented in parallel with other systems, allowing for higher loads, which would allow for adults to use these energy generating shoes. This would allow individuals such as hikers or military members with a much higher weight to charge batteries in their shoes while being off the grid without access to a power supply. The only problem with this theory is that multiple systems would take up significantly more space, leading to concerns with size management.

1.2.4. Fluid Energy Harvesting with Piezoelectric Materials (CFD)

In the scope of this project, CFD modeling is essential towards the advancement of the research. Currently there is a lacking of detailed research in the respective area. One area that addresses this is energy harvesting from a single cantilever beam with a cylindrical flow disruptor. An et al. and Zhao et al. have done research on this topic. In An et al.'s research, they study the Vortex-Induced Piezoelectric Energy Converter (VIPEC) system under a constant velocity and how the turbulence generated impacts the polyvinyl chloride piezoelectric material [19]. Their main focus is to determine how the length of the piezoelectric beam impacts the lift variables, which in turn impacts the voltage output and vibrational frequency. They utilize mathematical models of turbulence and 2D CFD simulations to verify their results, which indicates that a dimensionless length of 2 produces the most voltage. Unfortunately, since this is a relatively new concept, there is no physical results to compare to to further verify their data. However, Zhao et al. have also done a CFD analysis of the VIPEC model, adding a resistive load at the tip of the piezoelectric material to increase the vibrational frequency [20]. Their mathematical model is based on vibrational mechanics, with less of a focus on the governing equations of turbulence. Zhao's research utilizes COMSOL multiphysics, which allows for accurate modeling of fluid structure interactions, which is essential in modeling how turbulence impacts the behavior of the piezoelectric material.

A study that investigates multiple piezoelectric flow harvesters has been conducted by Lee et al., where an array of flow harvesters have been placed in a laminar flow and the turbulent interactions between them and the piezoelectric beam were observed in CFD [21]. In this study,

the energy harvesting piezoelectric material was not placed in the vibrating segments extruding from the plate, but instead within the plate where the vibrating extrusions transmitted the energy into them. This study consisted of turbulence inducers, where the non-piezoelectric material extrusions induced any necessary vibrations for the system to generate energy. It was observed that near the back of the array, the extrusions experienced low velocity flow, which would inhibit energy production from the piezoelectric material. The study relied on a symmetric design, which could have prevented ideal flow distribution from occurring. The researchers could have benefited from different design configurations, which would allow them to observe the ideal array distribution. This study is unique as it investigates multiple piezoelectric devices and how their behavior influences the other devices in the array.

1.2.5. Conclusion

The field of piezoelectricity has undergone much research in recent years. There are many options when it comes to what materials to work with and what the ideal energy-harvesting device is. Additionally, there are infinite possibilities for the application of these devices, and can be applied to virtually any system that undergoes frequent vibrations or mechanical stress. Fluid interactions is an excellent source of these vibrations, as the energy source is near infinite and can be placed virtually anywhere. There is a need for more research in the field of CFD and piezoelectric materials, especially for 3D interactions of multiple piezoelectric energy harvesters. Primarily, there is a need for physical tests to back the validity of the research that has been done using CFD.

1.3. Project Objective

The objective of this project is to optimize the design of flow disruptors to generate the most turbulent flow for a piezoelectric cantilever beam. The goal is to create a 2D CFD simulation of a flow disruptor and a piezoelectric energy harvester that will generate the maximum amount of energy in the given situation. The primary focus is to design and test multiple flow disruptors and determine which ones produce the highest amount of turbulent flow that is conducive for the piezoelectric materials. The second objective is to determine the optimal configuration of the piezoelectric cantilever beam that will harvest the most energy from the turbulent flow while minimizing the negative effects on the beam's structural stability.

1.4. Methodology

The initial goal is to investigate the performance of a piezoelectric beam with no flow disruptor in a 2D CFD simulation. From there, multiple 2D designs of flow disruptors will be tested and the optimal placement of a single piezoelectric beam will be determined. Lastly, power simulations will be ran to determine which configurations produce the most voltage and power.

2. Mathematical Model

The piezoelectric flow disruptor configuration is a heavily coupled system through both fluid and solid mechanics. Fluid mechanics dominate the first half of the system, with an assumed incompressible, laminar flow interacting with the walls and flow disruptor to generate turbulence. The turbulent flow then interacts with the piezoelectric beam, deflecting the beam due to the varying pressure forces of the turbulence.

2.1. Governing Equations

The inlet of the system assumes an incompressible, undeveloped, 2D laminar flow. Flow only exists in the horizontal x direction of the system, perpendicular to the flow disruptor. This inlet flow follows the Navier-Stokes equations of conservation of momentum and continuity, as shown in Eqs. 2.1 and 2.2.

$$\rho_f\left(\frac{\partial \vec{u}}{\partial \vec{t}} + \vec{u}_f \cdot \nabla \vec{u}_f\right) = -\nabla P + \nabla \cdot (\mu_f \nabla \vec{u}_f) \tag{2.1}$$

$$\nabla \cdot \vec{u}_f = 0 \tag{2.2}$$

At the inlet, the flow exists purely in the horizontal direction, allowing for all vertical flow variables of the Navier-Stokes equations to be removed. This allows for the momentum equations to be simplified into Eqs. 2.3 and 2.4, where 2.3 is the simplified x component, and 2.4 is the simplified y component.

$$\rho_f\left(\frac{\partial u_f}{\partial t} + u\frac{\partial u_f}{\partial y}\right) = -\frac{\partial P}{\partial x} + \mu\frac{\partial^2 u_f}{\partial y^2} \tag{2.3}$$

$$\frac{\partial P}{\partial y} = 0 \tag{2.4}$$

These equations allow for the initial conditions and overall behavior of the flow to be modeled in the simulation. In these equations, ρ_f refers to the density of the fluid, $\vec{u}_f$ refers to the velocity vector, P is the pressure, μ is the fluid viscosity, and u is the horizontal flow in the x direction.

The equations for the deformation of the piezoelectric beam are shown using Eqs. 2.5 and 2.6.

$$\rho_s \frac{\partial^2 \vec{u}_{solid}}{\partial t^2} = \nabla \cdot (FS)^T + \vec{f}_v \tag{2.5}$$

$$F = I + \nabla \vec{u}_{solid} \tag{2.6}$$

Any calculations performed assume the flow disruptor is a static beam, as any deformations are negligible regarding the fluid dynamics and compared to the deflection experienced by the piezoelectric beam. In Eqs. 2.5 and 2.6, ρ_s represents material density, $\vec{u}_{solid}$ represents displacement field, F is the deformation gradient tensor, S is the stress tensor, f_v is body forces, and I is the identity matrix.

The energy output of the piezoelectric beam can be generalized by Eqs. 2.7 and 2.8. While the equation is a simplified representation, it allows for a general understanding of the energy output with relation to the beam deflection.

$$D = dT + \varepsilon E \tag{2.7}$$

$$S = sT + dE \tag{2.8}$$

In Eqs. 2.7 and 2.8, D is the electric displacement, d is the piezoelectric coefficient, T is the stress, ε is the permittivity, E is the electric field intensity, S is the strain, and s is the elastic compliance. Piezoelectric coefficients are commonly denoted as d_{ij}, e_{ij}, g_{ij}, and h_{ij}. The most common coefficients for energy harvesting are d_{31} and d_{33}, so those will be the reference coefficients for equations 2.7 and 2.8.

3. Simulation Set Up

3.1. Introduction

The study of piezoelectric materials converting kinetic flow energy into electric energy is based on the study of deformation due to fluid structure interactions. The selection of software capable of these computations was critical due to this factor. Instead of using software that focused on fluid behavior, a software program that computed both fluid behavior and structural behavior was necessary.

The software selected for this project was COMSOL Multiphysics. The primary reason for selecting this software was due to its ability to perform both FEA and CFD simulations simultaneously. The secondary reason for its selection was its accessibility through the SJSU remote desktop.

3.2. Software Validation

3.2.1. Goals

The validation objective for this software is to show that it is capable of simulating a vibrating piezoelectric beam with no flow disruptor. There were two main characteristics being looked for. The first was the oscillation of the piezoelectric beam over a set period of time. If the software could simulate the vibration of a piezoelectric beam in a steady flow, it would be possible to simulate more complex geometries and their resulting flows. The second characteristic being looked for was the development of pressure differences behind the beam, or turbulence. Turbulence generated from laminar flow was critical in this study, so it was essential to check if turbulence could be generated from a simple geometry.

3.2.2. Geometry

The geometry being used in this validation study was a simple beam fixed to a flat geometry in 2D. This configuration was a simplified version of the final 2D configuration with a flow disruptor and a piezoelectric beam. Figure 3.1 illustrates the design of this geometry. The domain was 100 mm wide by 20 mm tall, and the piezoelectric beam was 0.2 mm wide and 8 mm tall. Since this was a validation study, the geometry was not identical to today's current piezoelectric beams. However, the thickness-to-length ratio was on the more conservative side, so a more accurate geometry would yield better results.

Figure 3.1 - Validation geometry

3.2.3. Mesh

In this study, the fluid and solid domains were created using a 2D triangular mesh with 61,761 domain elements and 1,781 boundary elements. This mesh was generated using the automatic mesh feature in COMSOL, so further refinement was necessary. Additionally, this size was based on a mesh convergence study, with this mesh size being the most refined. The mesh convergence study looked at the root mean square of the tip displacement of the single beam over a wide variety of meshes from extremely coarse to extra fine. Figure 3.2 illustrated the results of this study, where positions 7 and 8 yielded similar results, indicating a point of diminishing returns. Since more detailed meshes take significantly longer to simulate than coarser ones, the least detailed mesh that yielded similar results was ideal. Figure 3.3 shows the entire mesh at extra fine settings with Figure 3.4 showing the mesh at the top end of the piezoelectric beam. A moving mesh was set as well to take into account the deformation of the beam.

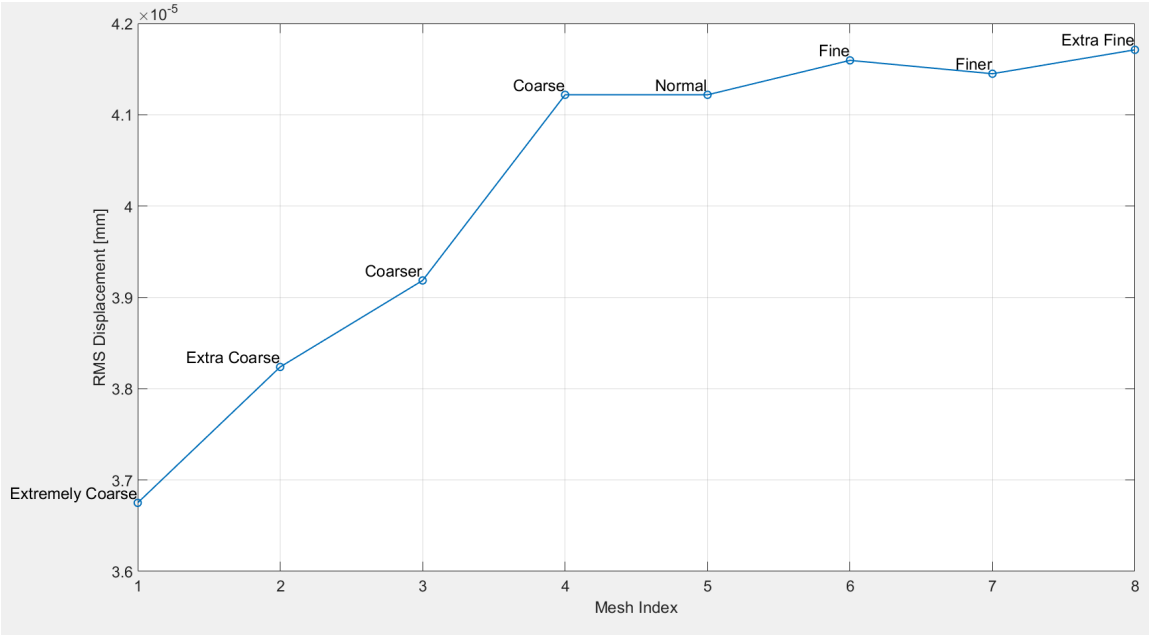

Figure 3.2 - Mesh convergence study

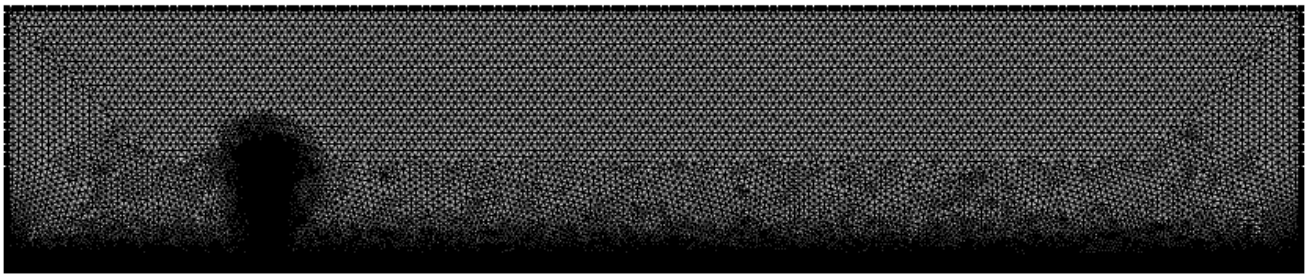

Figure 3.3 - Mesh total

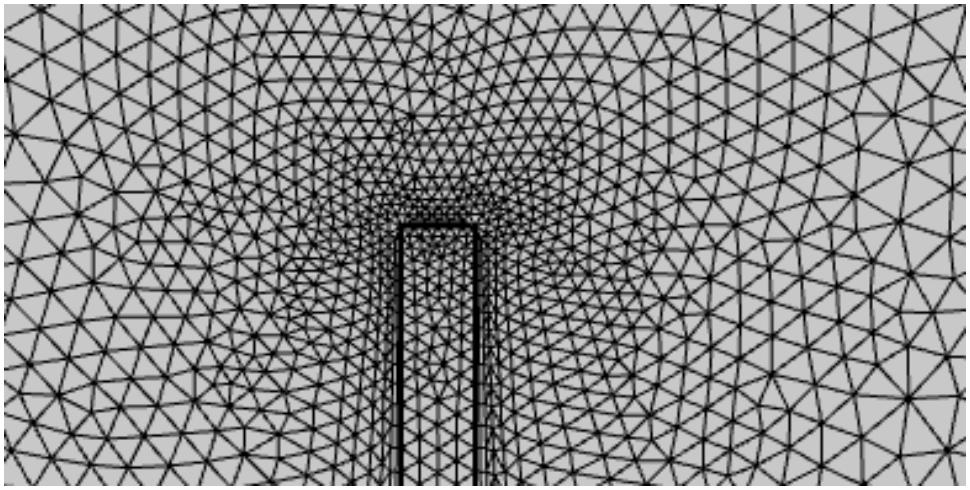

Figure 3.4 - Mesh beam top

3.2.4. Physics Modeling

In this validation, various physical settings are designated. When defining the fluid flow characteristics, laminar flow models were used to predict the flow behavior. In the case that a RANS turbulent flow model was used, the flow behind the beam would be averaged and not yield the desired pressure distributions. Therefore, a laminar flow model was used in this simulation. Additionally, the version of software used for this study did not include a turbulence module, leading to the choice of laminar flow. All the fluid properties were taken for air at standard sea level conditions, with the main components being the density set to 1.225 kg/m^3 and viscosity set to $1.81e^{-5}$ Pa*s. No initial values were set for the fluid domain, as the system was observed as time progressed in an initially stationary system. Since the system was being simulated as a fixed geometry with an infinitely large domain, the bottom geometry and structure were set to no slip while the top wall was set to slip conditions. The inlet of the domain was set to be a velocity-dependent flow, where the max velocity was set to 1.4 m/s and multiplied by a step function to gradually increase the velocity over 0.1 seconds to not overwhelm the simulation. The outlet of the system was set to the opposite side of the inlet, with the pressure option selected for the boundary conditions. Pairing the pressure boundary condition with suppressed backflow, excess flow from outside the domain was prevented from flowing in.

The solid mechanics physics was a two part process of defining material properties and specifying geometry boundary conditions. The materials were assumed to be isotropic for ease of calculations, making Young's modulus, Poisson's ratio, and density important variables for defining the material behavior. These three values were manually imputed as the material library did not have the material properties for Lead Zirconate Titanate (PZT-5J). No initial values were added to the beam of the system, as the point of the study is to observe how it behaves from interaction with the flow alone and with no outside influence. The last variable added to the solid mechanics tab was a fixed condition, which was set at the connecting point between the beam and the domain boundary. A tab for free variables was automatically set by the software, but no unassigned variables existed in this simulation.

The last section to define was the multiphysics tab, which was where the fluid structure interaction (FSI) was defined. In this section, the boundaries that interacted with both the fluid and structure were selected, which were the walls of the beam. The fluid and structure domains

were selected as well, which were the aforementioned laminar flow model and the solid mechanical model. The fully coupled geometry option was selected, as the study looks to see how fluid flow impacts solid structure behavior and vice versa.

Other variables were then defined after those that were not physics related but important to obtaining results, such as domain point probes and animations of velocity, pressure, and deformation.

3.2.5. Results

In the most refined simulation case, both deformation and turbulence were observed. The behavior of the beam was shown through both animation and the use of a domain point probe. In the animation, the beam could be seen oscillating with a direct correlation to the intensity of the inlet flow. The domain point probe gave a more accurate numerical value to the oscillations. It was observed to gain higher and higher deflection as the inlet velocity increased, then oscillating once the velocity became constant (Figure 3.5). While the magnitude of oscillation was relatively small, once the size of the beam was increased and a proper flow disruptor was created, much larger deformations were expected.

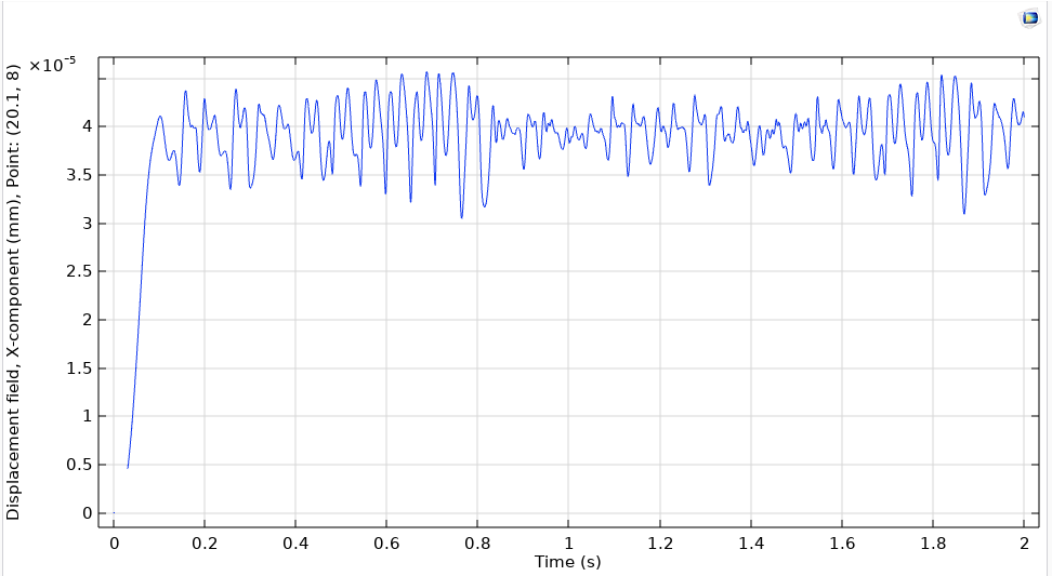

Figure 3.5 - Deformation of free beam

The other aspect that was observed in this validation experiment was the development of pressure differences behind the piezoelectric beam. In lower refinements, no turbulence was observed, resulting in virtually no pressure differences behind the beam once the flow speed stabilized (Figure 3.6). However, in higher refinements, the development of turbulence was shown early on and continued to be seen as the simulation ran. This was evident in areas of low and high pressure, and the more refined the mesh became, the more turbulence was observed (Figure 3.7). These refinements reached a point of convergence around the finer mesh setting. After the finer mesh setting, there was no change in the details of the turbulence.

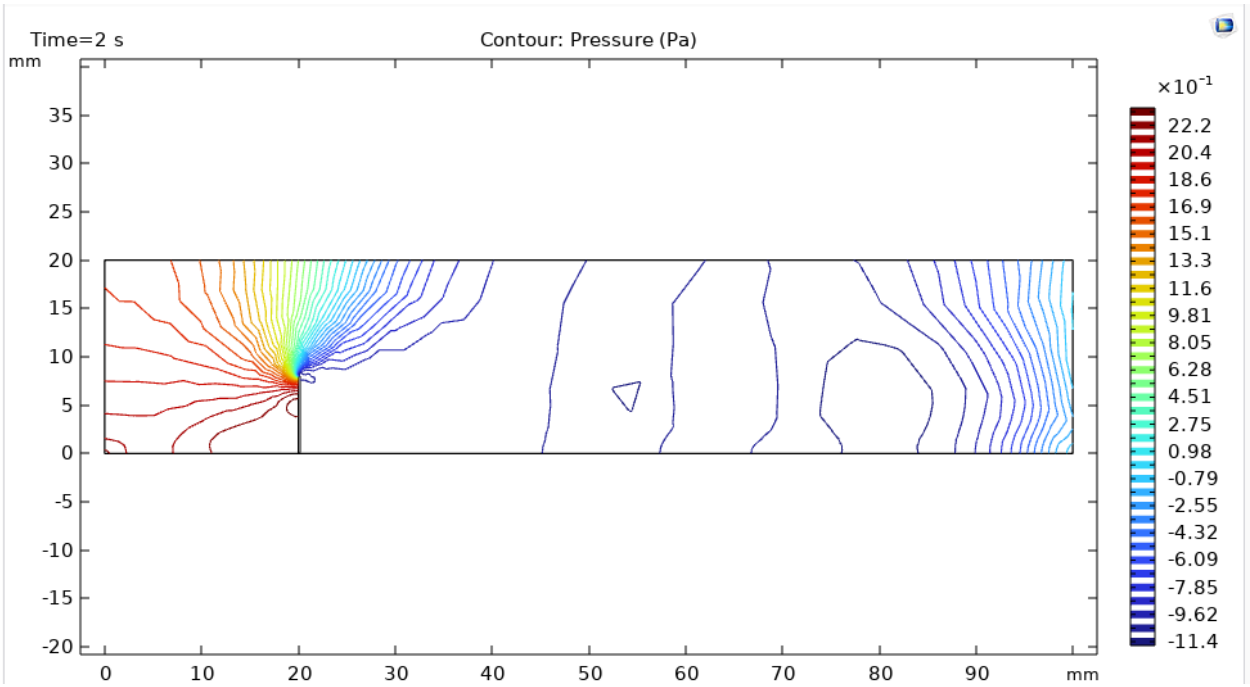

Figure 3.6 - Low refinement pressure distribution

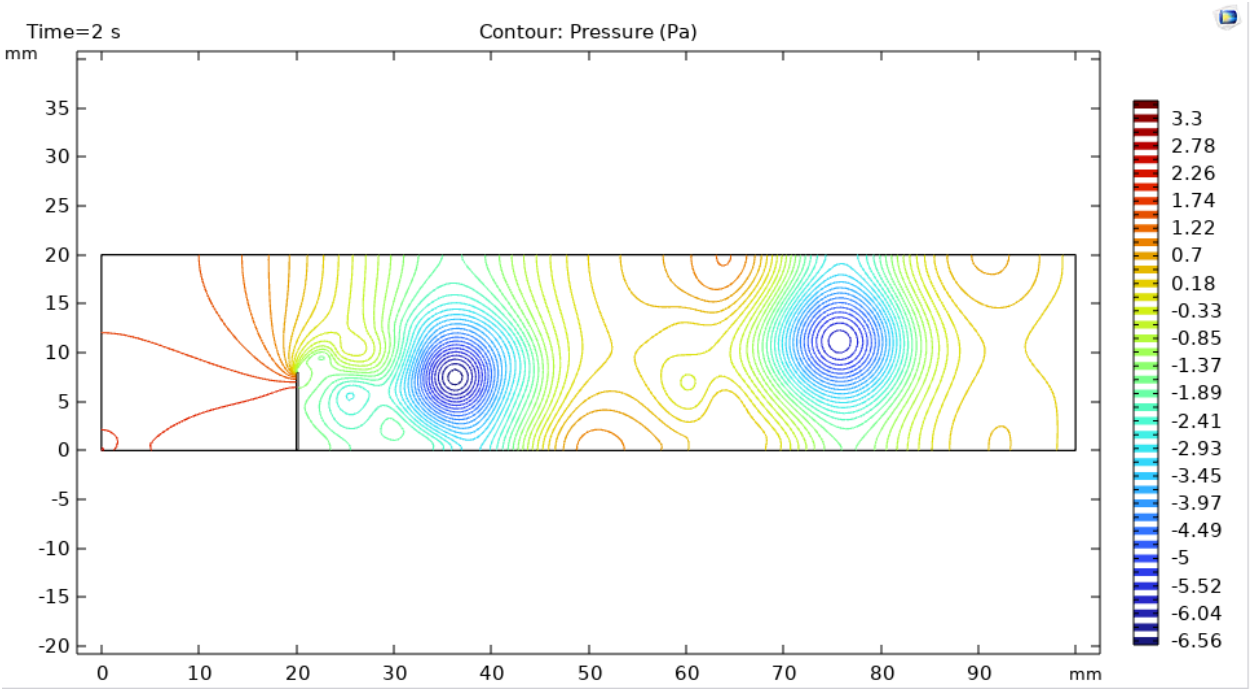

Figure 3.7 - High refinement pressure distribution

4. Results

4.1. Sizing and Spacing

One of the most important objectives of this study was to observe how the positioning and sizing of the flow disruptor impacted the behavior of the downstream piezoelectric beam. The size of the piezoelectric beam was set to a commercially available beam size of 54 mm tall and 0.46 mm wide. The position of the beam was simulated in six different locations, from 200 to 700 mm away from the flow disruptor, with each successive position increasing by 100 mm. The other variable, the size of the flow disruptor, was simulated in 5 different configurations: a third the size, half the size, the same size, double the size, and triple the size of the piezoelectric beam (18, 27, 54, 108, and 162 mm). Simulations were performed with each individual configuration, leading to a total of 30 simulations to explore how each variable interacted with each other and how that impacted the overall performance of the piezoelectric beam.

Additionally, adjustments were made to the simulation set up to accommodate the more complex system seen in this section. The size of the domain was increased to 1200 mm to more accurately simulate the infinitely large domain above the system that will be seen in practical applications. A flow disruptor was also added to this configuration. The flow disruptor was set to be structural steel, as it is infinitely rigid in comparison to the piezoelectric beam. A more detailed mesh was constructed to accommodate the more complex system. Instead of using the computer-generated, physics-controlled mesh, a custom mesh was implemented. This mesh consisted of 10,115 domain elements and 351 boundary elements. The base size of the mesh remained at the finer setting per the mesh refinement study (Figure 3.2). The air domain was then precalibrated to fluid dynamics instead of general physics, with a fine mesh setting. An extra fine boundary mesh was then created along each solid surface to improve mesh resolution near the deflecting beams. The resolution of the beams was then increased, creating a grid pattern with two distribution meshes. Next, a corner refinement was added to decrease the mesh sizes at sharp corners in the study. A boundary layer mesh was then applied to all surfaces with two layers and a stretching factor of 1.2. Lastly, a free triangle mesh was applied to all remaining geometric entities. Through the implementations of these changes, the simulation was able to run properly without having to apply an extra fine mesh to the entire system. Figure 4.1 shows an up close look at one of the beams and the surrounding mesh.

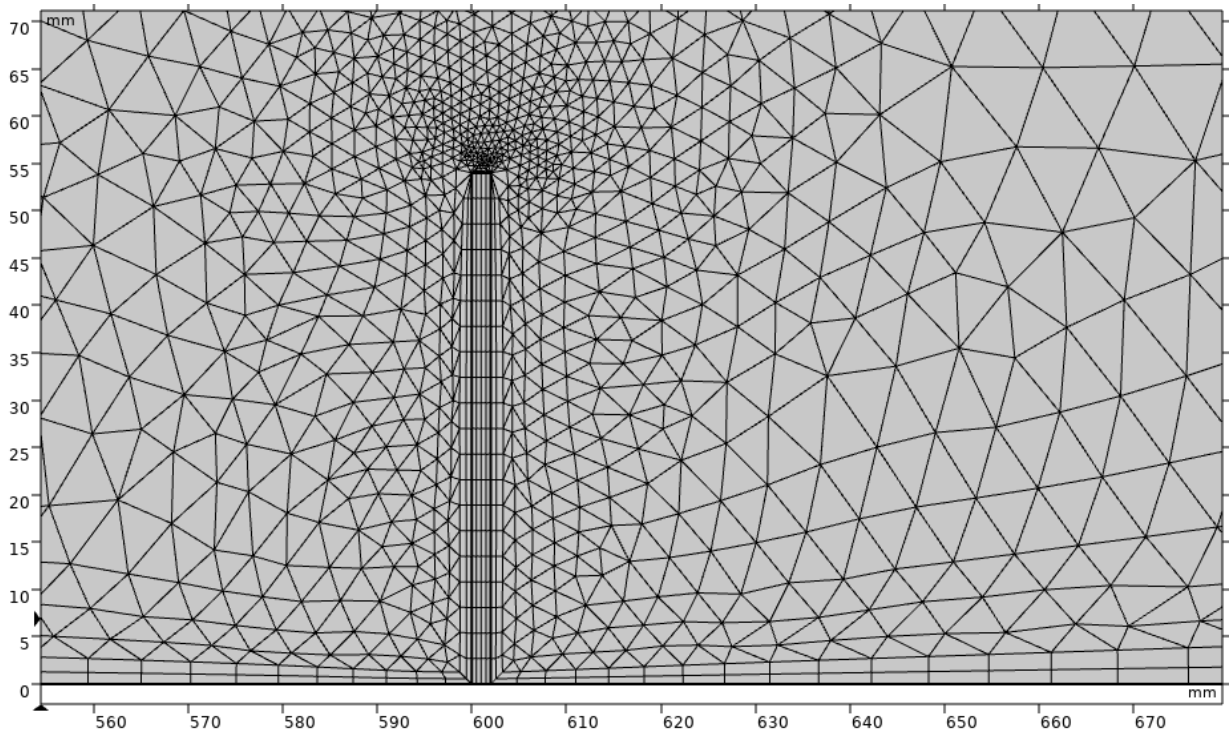

Figure 4.1 - Updated mesh

The last change that was made was an increase in maximum iterations. The default for maximum iterations was set at 20, which did not allow the system to converge when it became more complex. By increasing the max iterations to 100, the simulation took longer to run but was able to reach convergence and simulate the full 10 seconds.

4.1.1. Beam Displacement Behavior

The behavior of the piezoelectric beam could be categorized into four categories: erratic deflections, converging to zero, erratic oscillations, or predictable oscillations. Figure 4.2 categorizes the four possible behaviors in a chart, with the top row categorizing the size of the flow disruptor and the left column categorizing the distance between the disruptor and the piezoelectric beam. In both cases, the smaller the reference number, the smaller the scalar value (i.e. 1 in the top row is 18 mm or 6 in the left column is 700 mm). For example, (1,3) refers to a disruptor height of 18 mm and a gap of 400 mm. In the figure, blue categorizes models that converged to zero, red categorizes erratic deflections, green categorizes oscillatory behavior, and red/green categorizes erratic oscillatory behavior. Examples of each behavior can be seen in Figures 4.3-4.6.

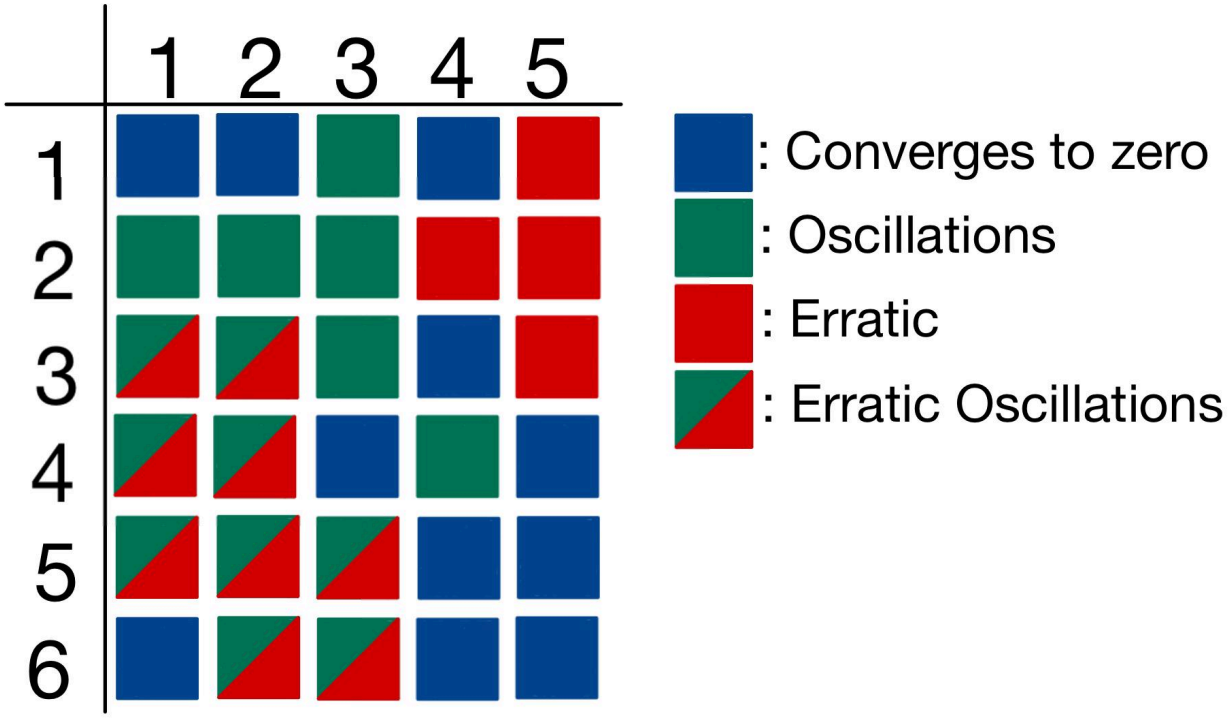

Figure 4.2 - Various geometry behaviors

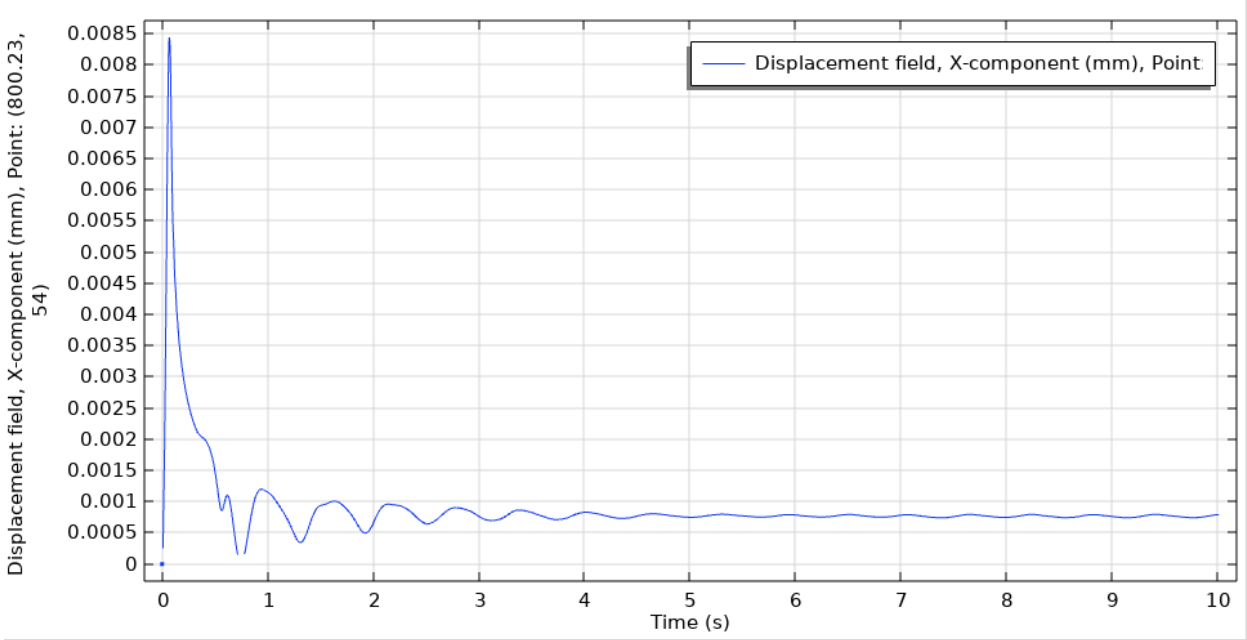

Figure 4.3 - Converges to zero

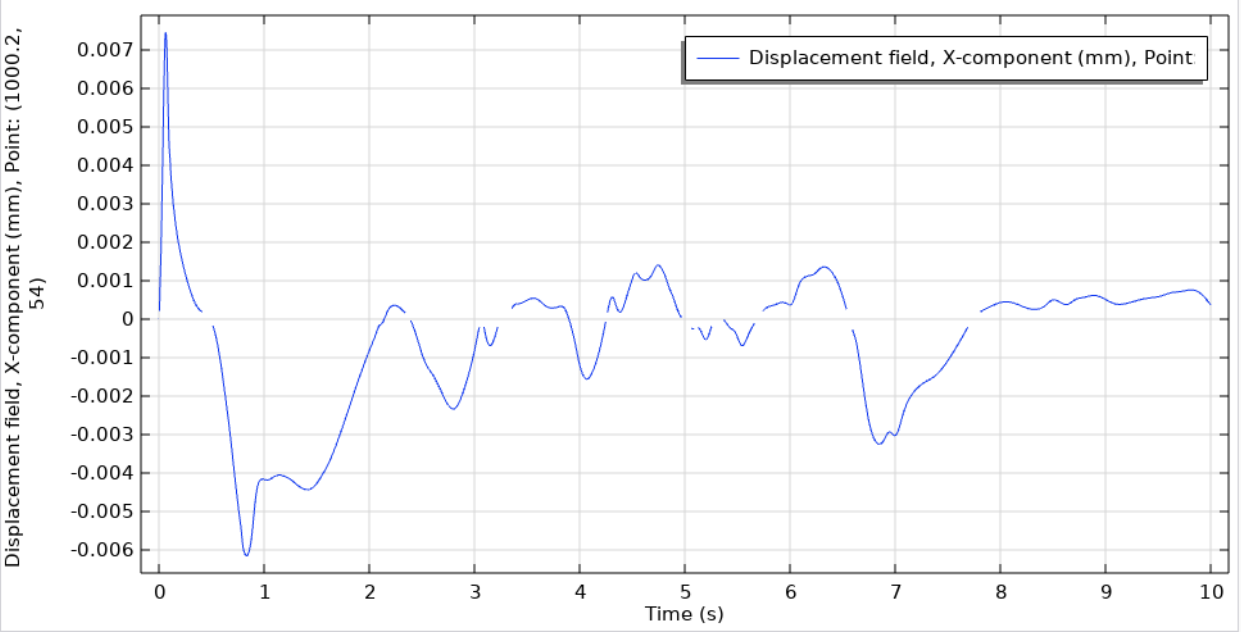

Figure 4.4 - Erratic deflections

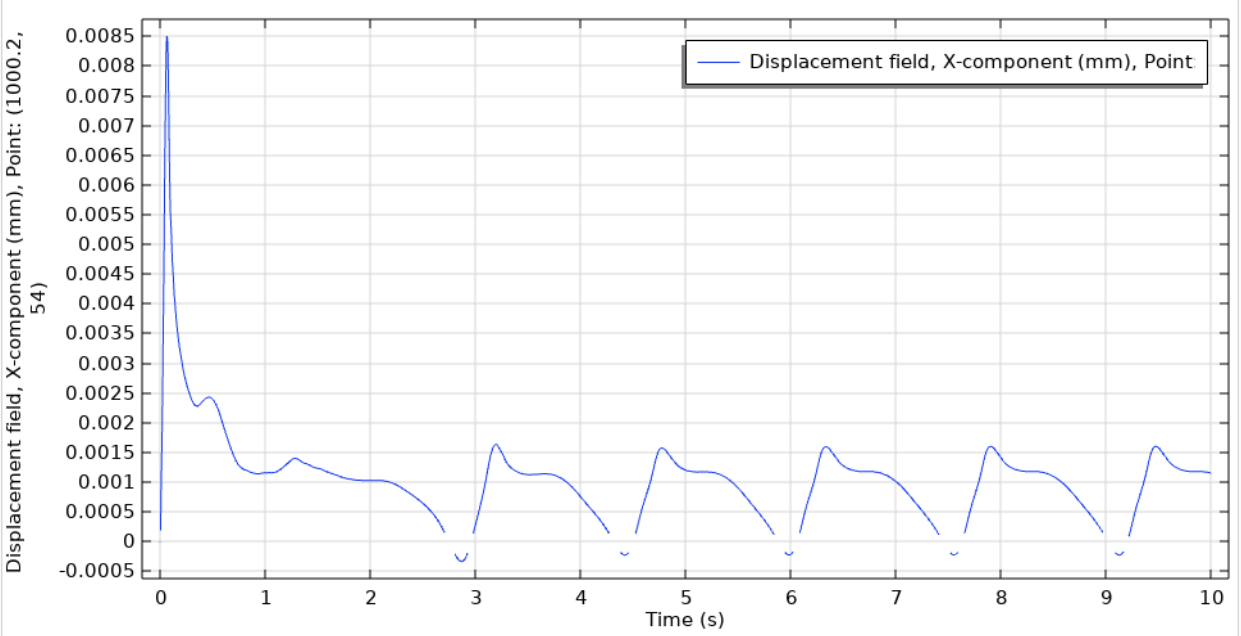

Figure 4.5 - Erratic oscillations

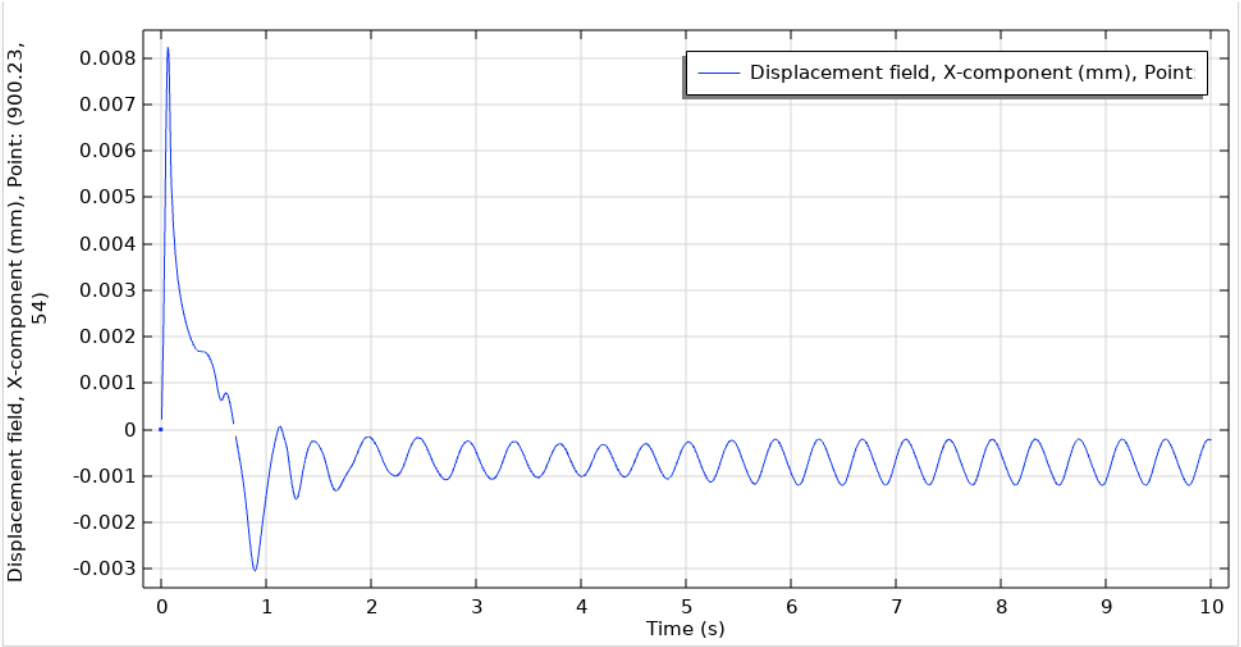

Figure 4.6 - Predictable oscillations

For the purpose of this study, predictable oscillations were the desired output for the simulations. While erratic oscillations gave larger ranges of displacement, the behavior was less predictable. Additionally, the energy output of the predictable oscillations produced more desirable results than the erratic oscillations, which can be seen later in this report. It can be seen that when the flow disruptor is 54 mm or less, or the distance between the disruptor and piezoelectric beam is 400 mm or less, erratic deflection behavior is produced with some exceptions. In the case that these conditions are both met, predictable oscillations are produced with some exceptions. These oscillations had a smaller amplitude than the erratic oscillations but had a much higher frequency. The amplitudes in the two cases were approximately three times larger in the erratic oscillations, and the frequency was approximately three times smaller compared to the predictable oscillations. Figures 4.7-4.12 show the six geometries that yielded the predictable oscillations.

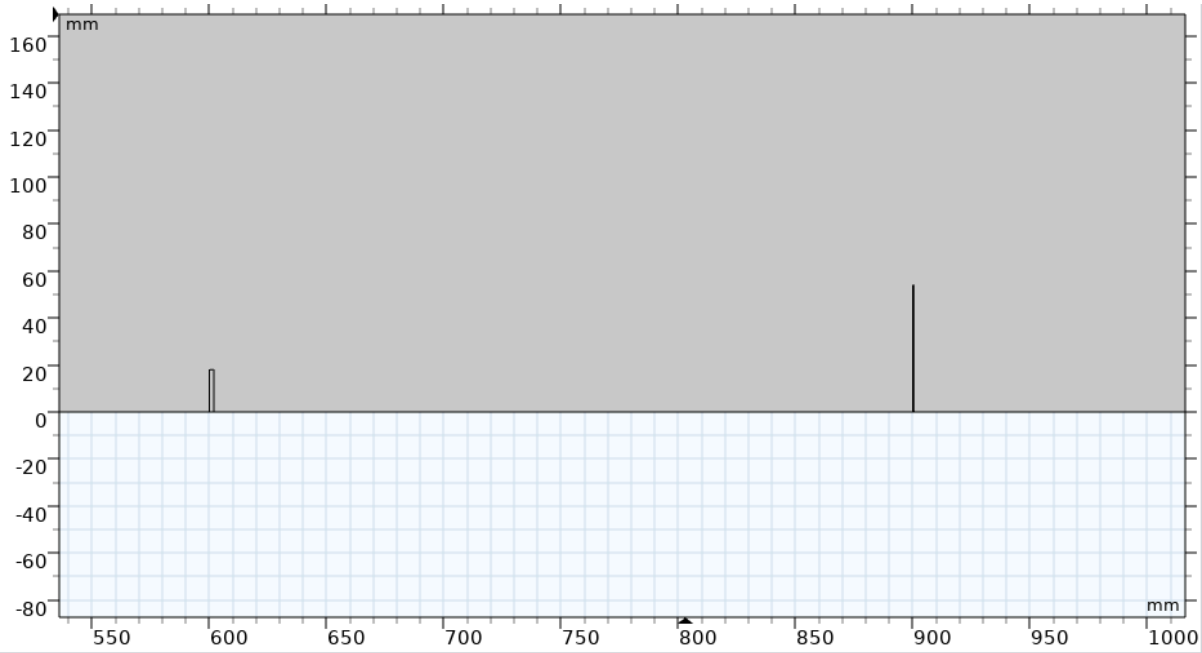

Figure 4.7 - Height: 18 mm, distance: 300 mm

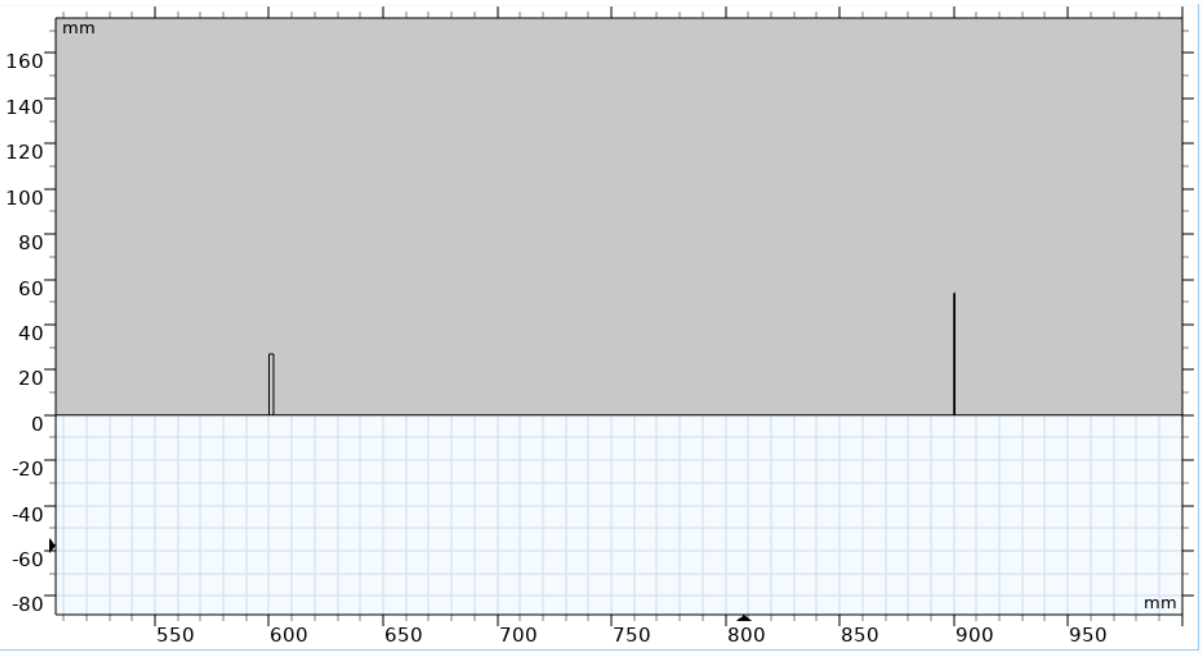

Figure 4.8 - Height: 27 mm, distance: 300 mm

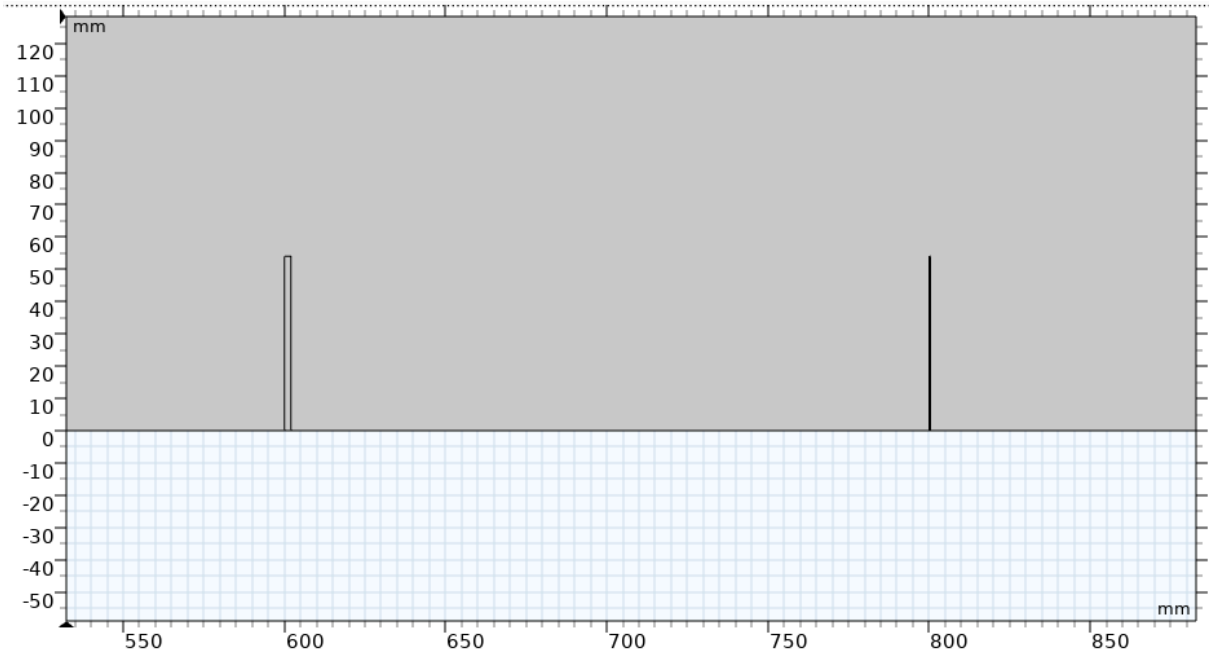

Figure 4.9 - Height: 54 mm, distance: 200 mm

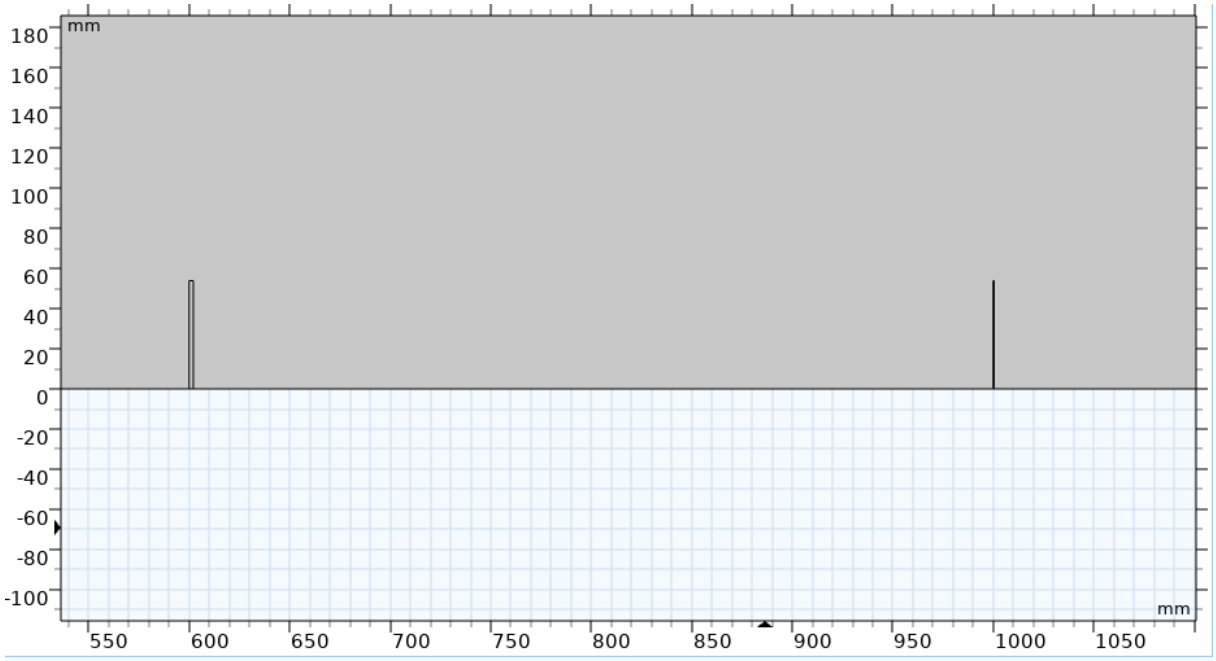

Figure 4.10 - Height: 54 mm, distance: 400 mm

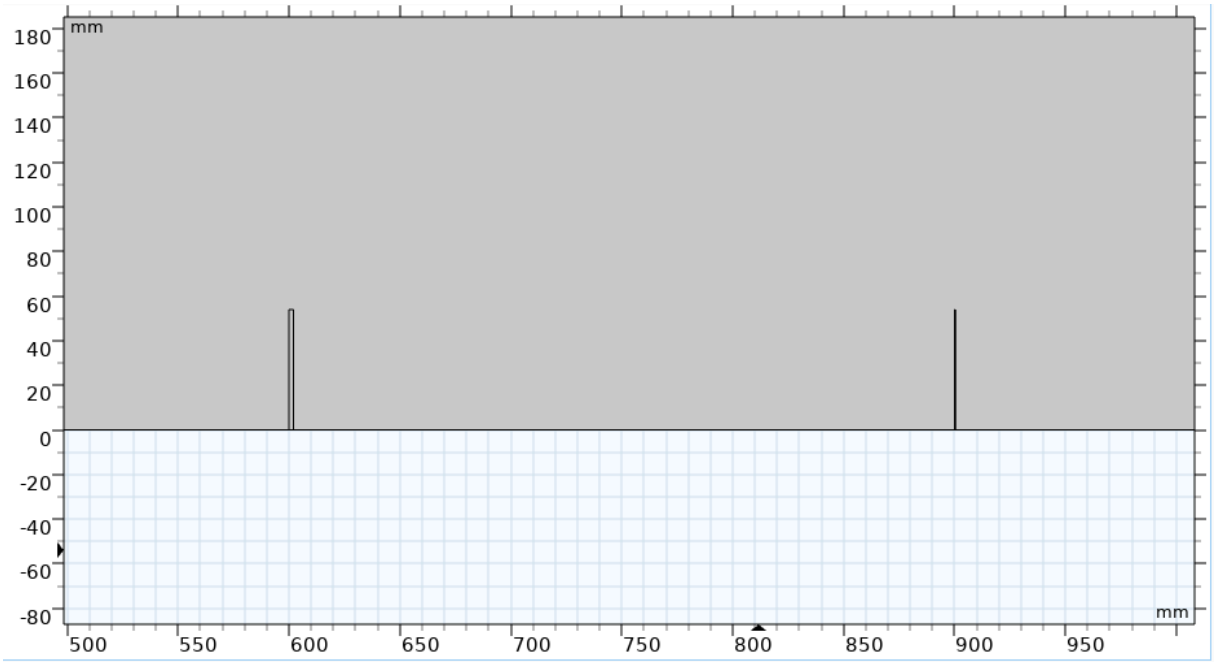

Figure 4.11 - Height: 54 mm, distance: 300 mm

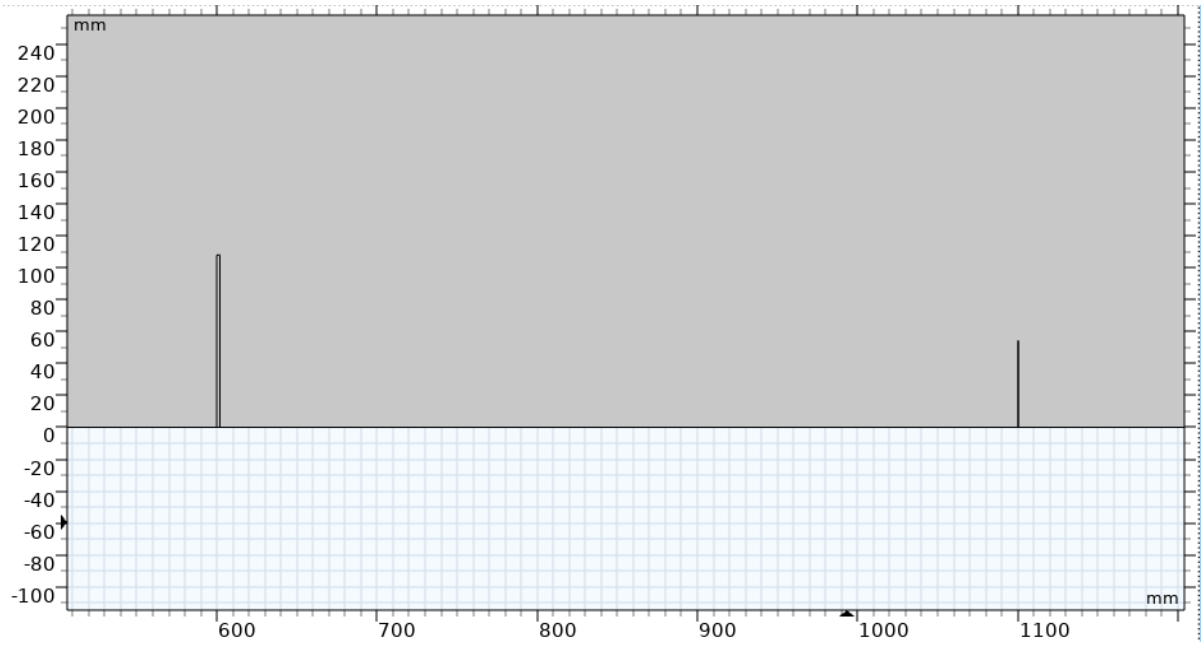

Figure 4.12 - Height: 108 mm, distance: 500 mm

The six configurations that produced the predictable oscillatory behavior all have similar characteristics, with the flow disruptor being fairly close to the size of the piezoelectric beam. In half of the cases, the disruptor was the exact size of the piezoelectric beam at 54 mm tall. The distance between the two was also relatively small, with the only case of it being notably larger in Figure 4.12, which has a larger disruptor as well. The behavior of this configuration barely qualifies for oscillatory, so this configuration is the upper limit of what produces reliable oscillations. The most reliable configurations for oscillations were Figures 4.8-4.11, which

consisted of flow disruptors no larger than the size of the piezoelectric beam and distance no larger than 400 mm between the two beams.

4.1.2. Pressure and Velocity

The pressure and velocity of the systems were the essential variables that determined the behavior of the beams as seen above. For the sake of consistency, the same systems that were used in the examples will be the four representations of each category of the 30 simulations ran.

In simulations that converged to zero, the predominant issue was the inability of the flow disruptor to generate velocity and pressure differences and have them interact with the piezoelectric beam. In the cases where the flow disruptor was larger than the piezoelectric beam, the larger flow disruptor essentially blocked the flow from interacting with the piezoelectric beam. In the other cases, such as the gap or the disruptor being too small, there was not enough room for turbulence to generate so that it could interact with the piezoelectric beam. Figures 4.13-4.14 show velocity and pressure distribution in a stabilized flow (8 seconds).

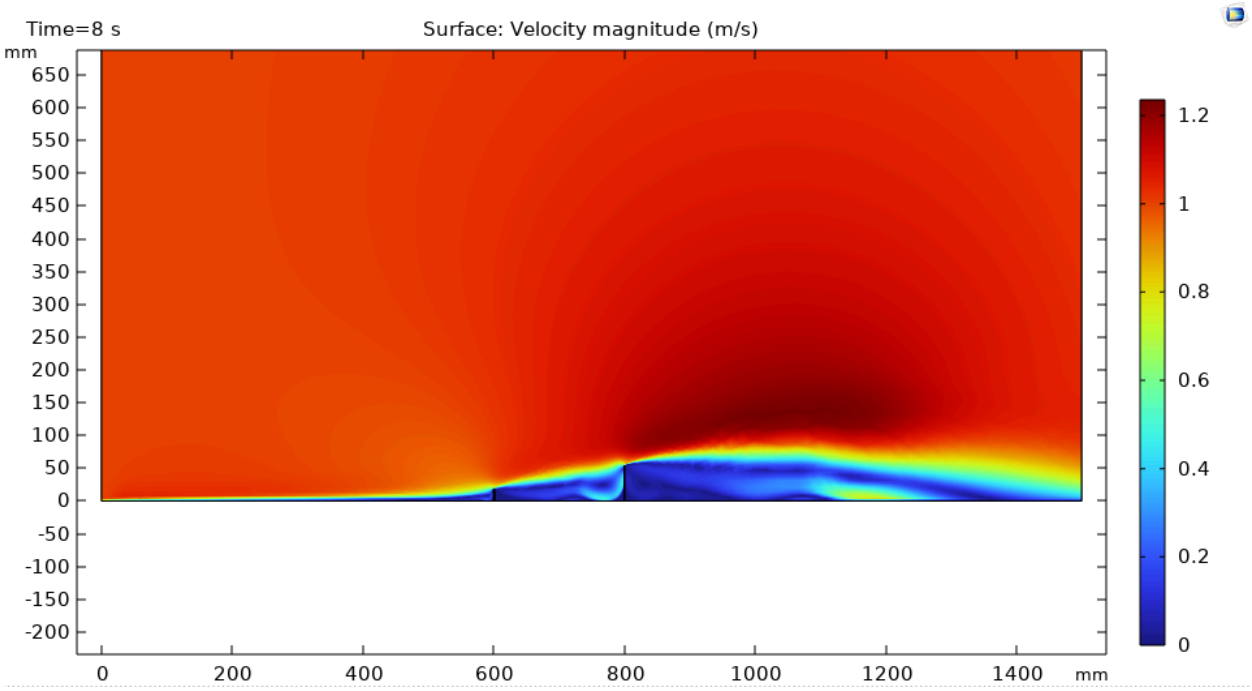

Figure 4.13 - Zero convergence velocity

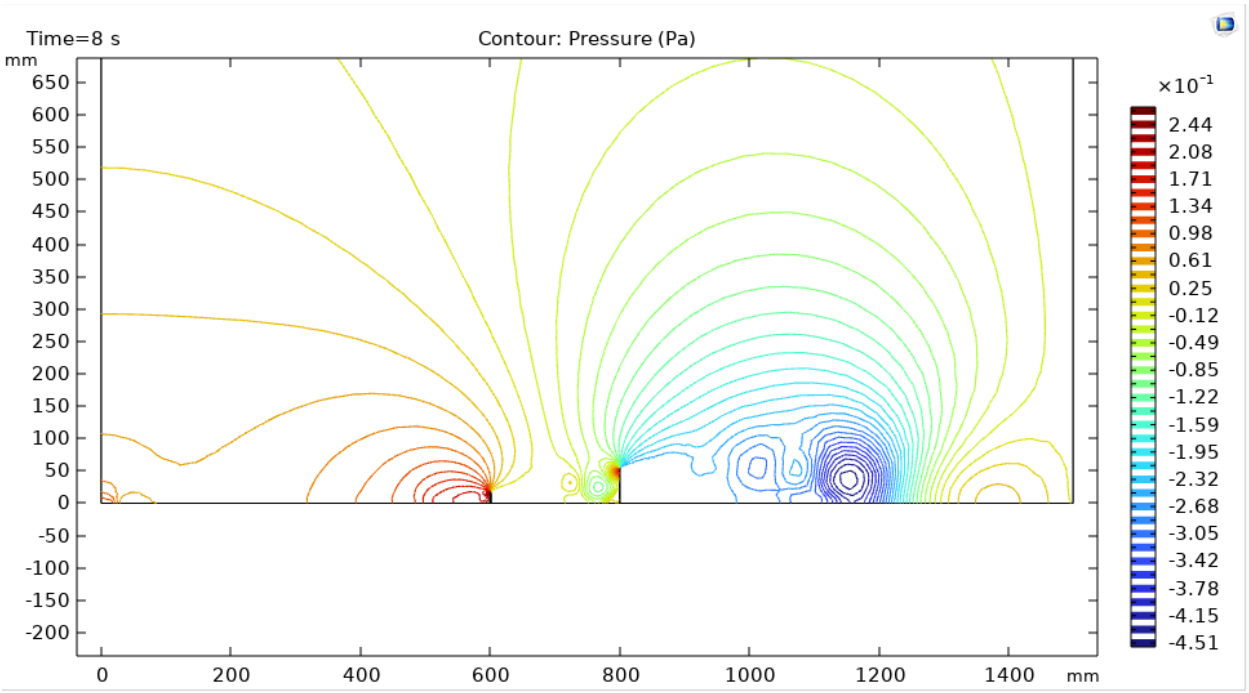

Figure 4.14 - Zero convergence pressure

When observing the velocity profile of Figure 4.13, the flow never gets the chance to speed up between the disruptor and the piezoelectric beam. The only time it speeds up is at the base as it begins to interact with the beam, but never to develop turbulence. However, downstream of the piezoelectric beam, the flow can speed up and develop some pressure differences. Looking at the pressure distributions in Figure 4.14 confirms what is seen in Figure 4.13. There are little pressure differences between the two beams and the difference only develops downstream when the flow has time to speed up and become turbulent. The gap between the beams is too small and prevents any significant fluid structure interactions from occurring.

In cases where the behavior of the piezoelectric beam is erratic displacement, there is a significant amount of turbulence interaction. In all of the cases, the flow disruptor was at one of its largest size configurations while the piezoelectric beam was relatively close. This placed the piezoelectric beam in the most turbulent zone where the flow was generating significant pressure differences after interacting with the flow disruptor. Figures 4.15 and 4.16 show the changes of pressure over two seconds while Figures 4.17 and 4.18 show the same thing with velocity.

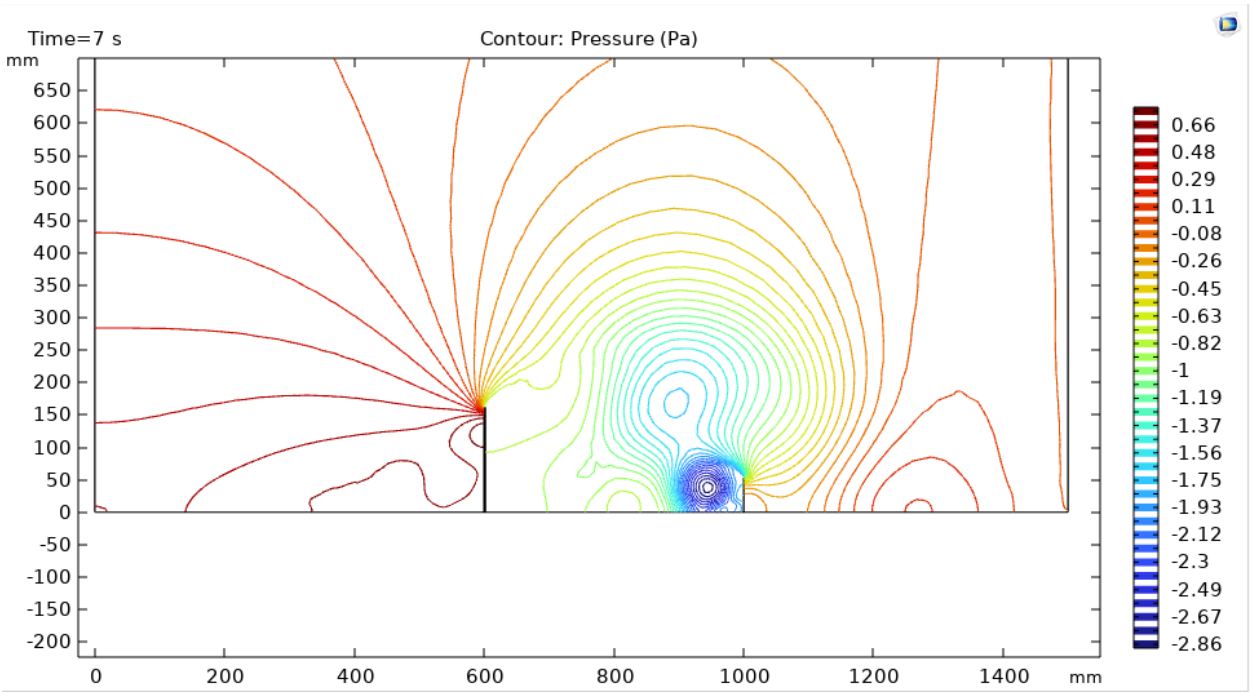

Figure 4.15 - Erratic deflections pressure 7 seconds

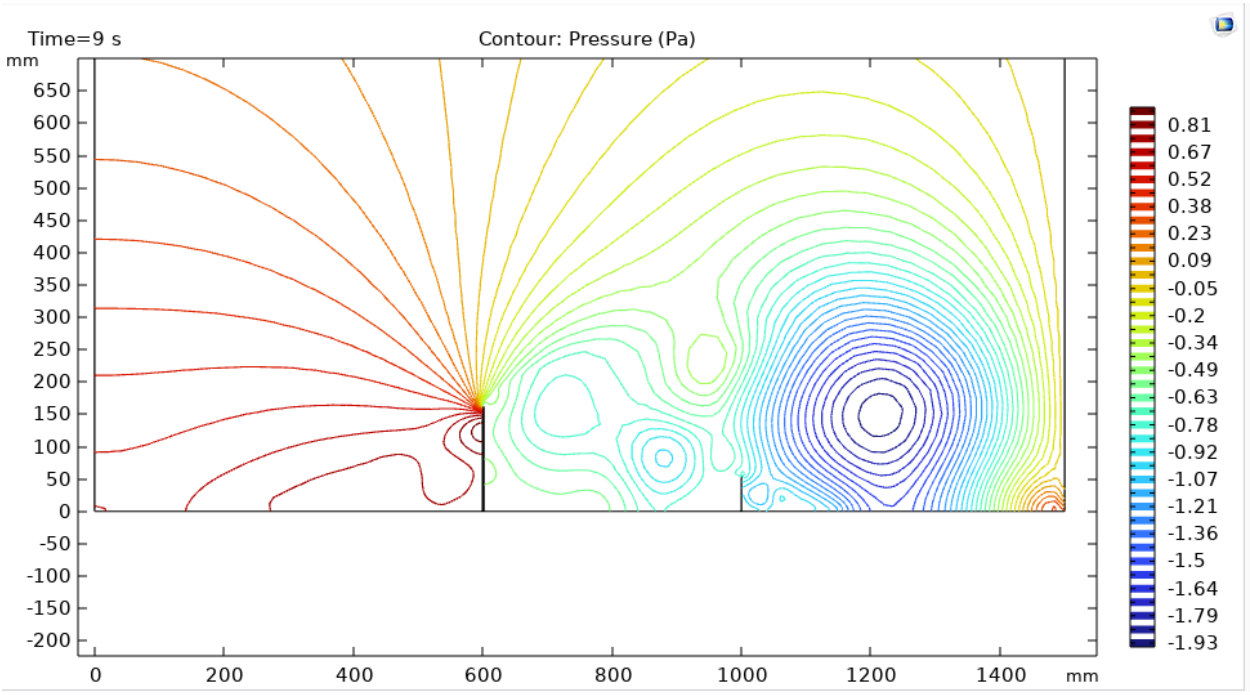

Figure 4.16 - Erratic deflections pressure 9 seconds

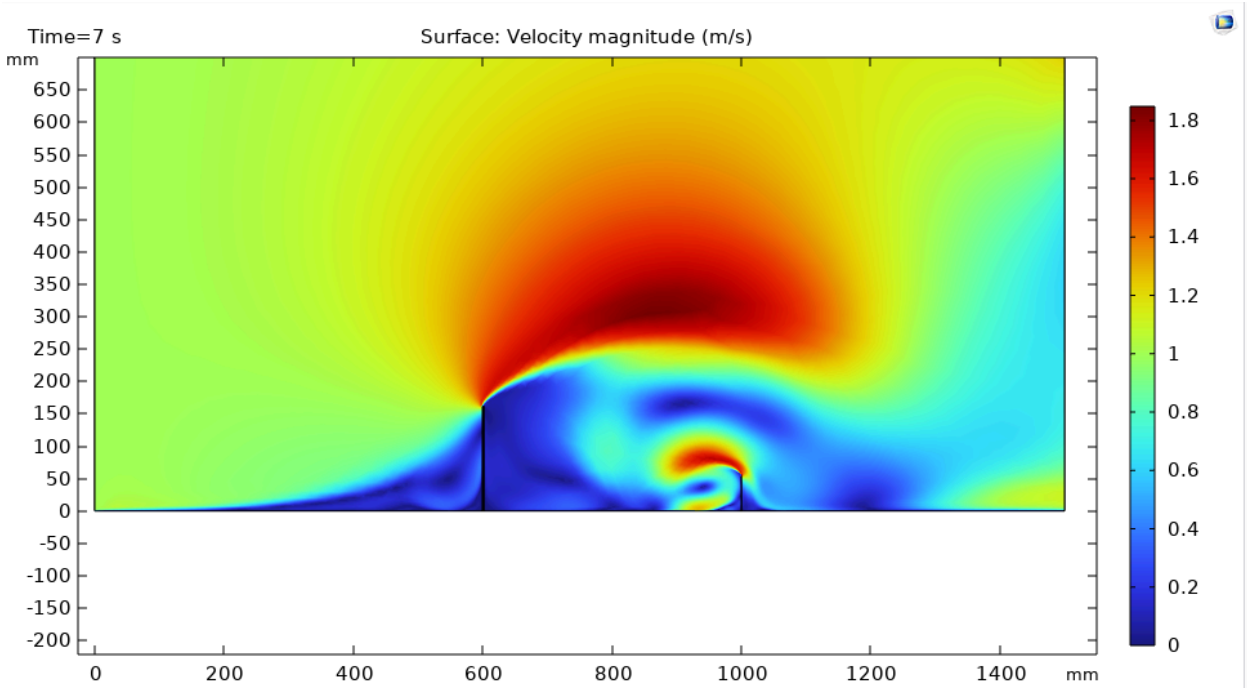

Figure 4.17 - Erratic deflections velocity 7 seconds

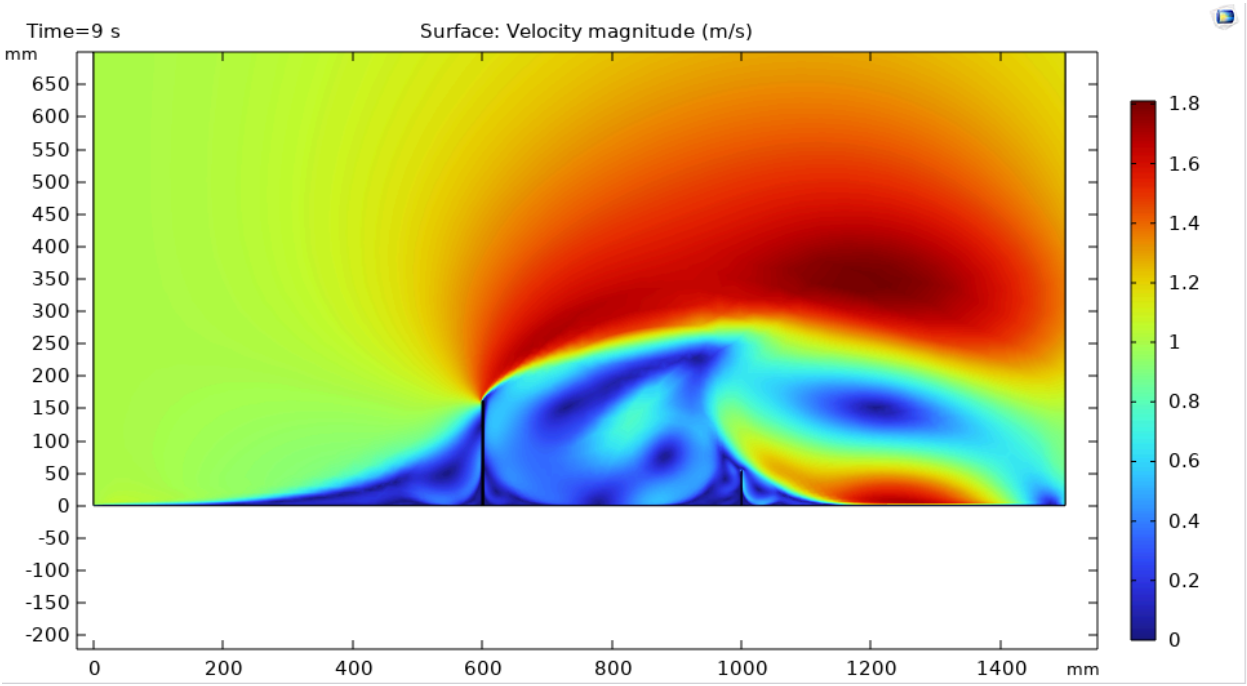

Figure 4.18 - Erratic deflections velocity 9 seconds

In both the velocity and pressure case, after two seconds the difference is significant. This constant shifting of forces on the piezoelectric beam caused large, unpredictable changes in its displacement. While large changes result in higher electric output, it makes it difficult to track the efficiency of the flow disruptors, making it an undesirable configuration for the purpose of this study.

The erratic oscillations occurred in cases where sections of high velocity crest off the top of the flow disruptor and impact the piezoelectric beam. This is seen in the configuration where the flow disruptor is relatively small and there is a somewhat significant distance between the two beams. The interaction behaves similarly to waves crashing against an object for the velocity or areas of low pressure hitting the beam for the pressure. Figures 4.19 and 4.20 show the interaction of the pressure on the piezoelectric beam, while Figures 4.21 and 4.22 show the interaction of velocity on the piezoelectric beam over 0.4 second period.

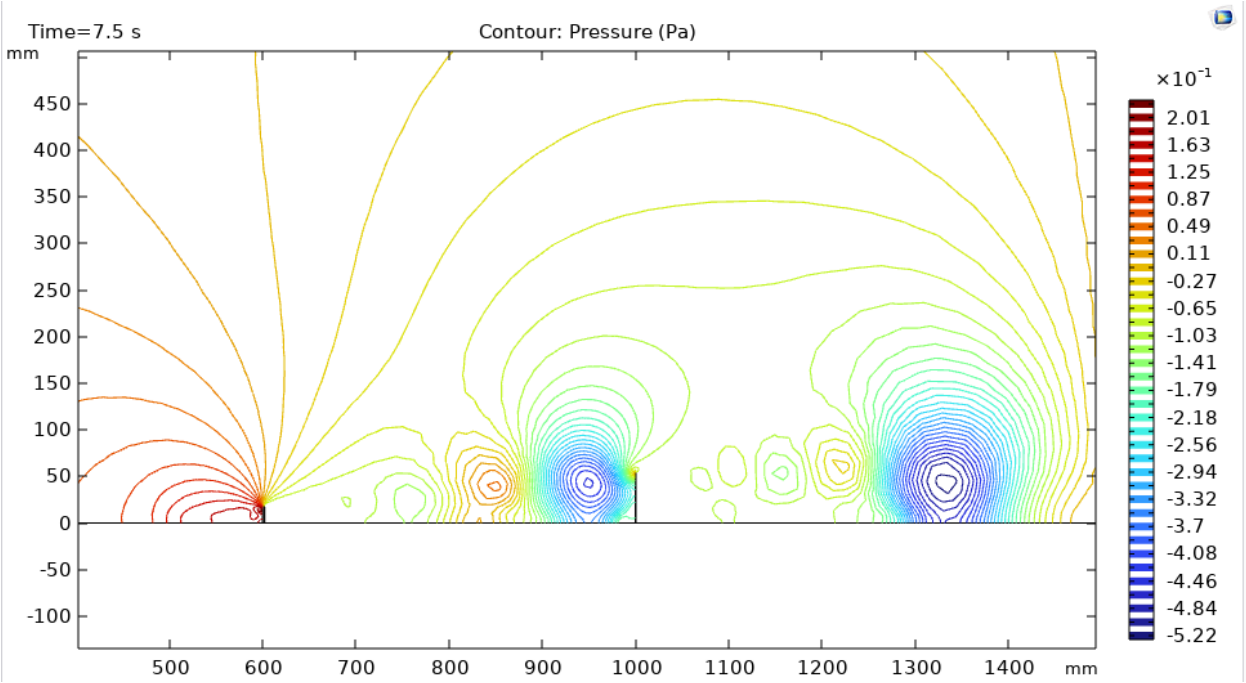

Figure 4.19 - Erratic oscillations pressure 7.5 seconds

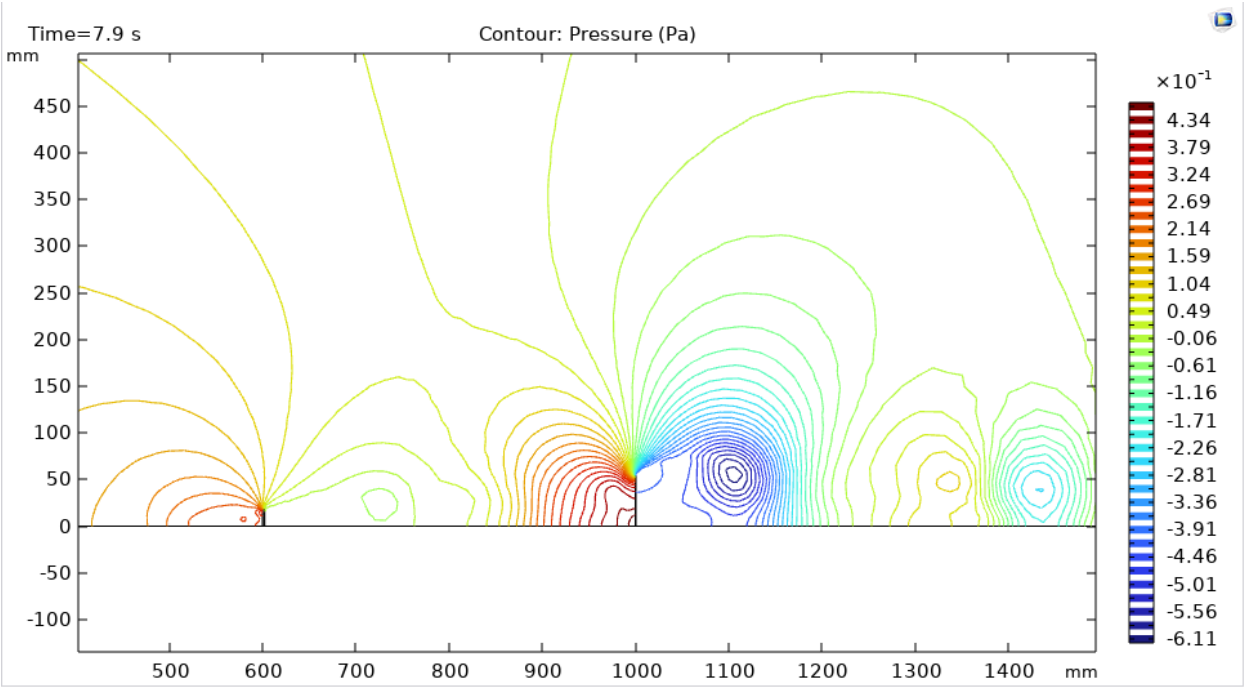

Figure 4.20 - Erratic oscillations pressure 7.9 seconds

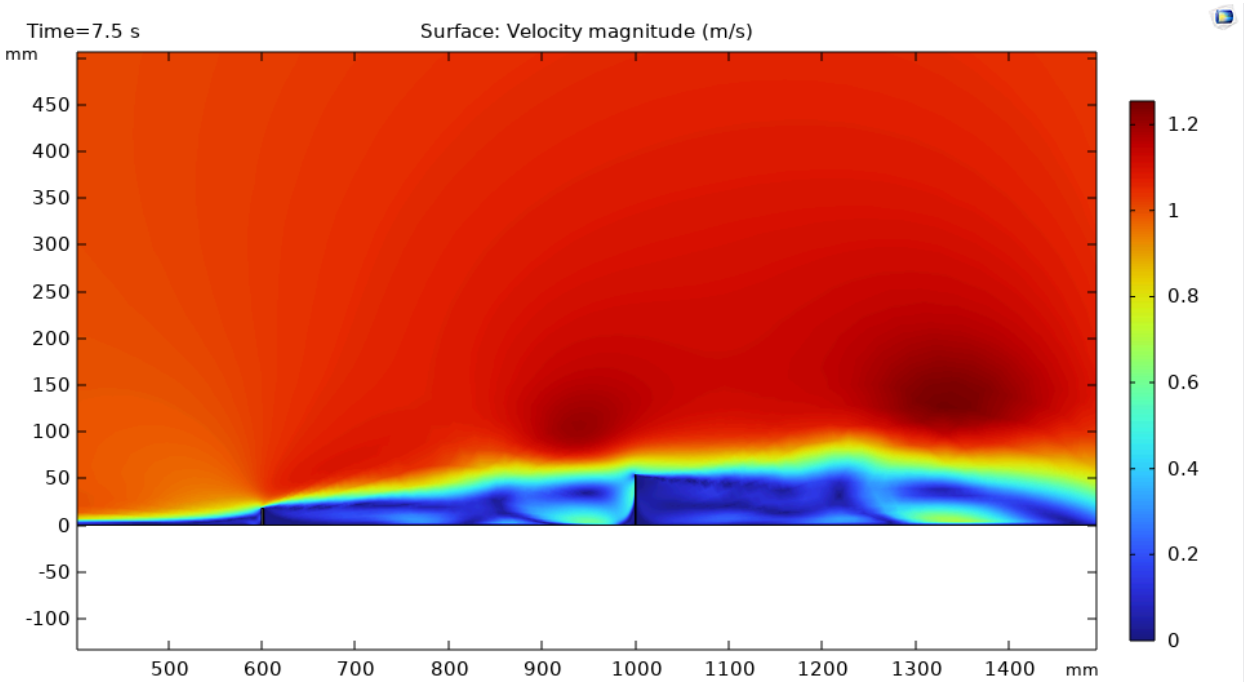

Figure 4.21 - Erratic oscillations velocity 7.5 seconds

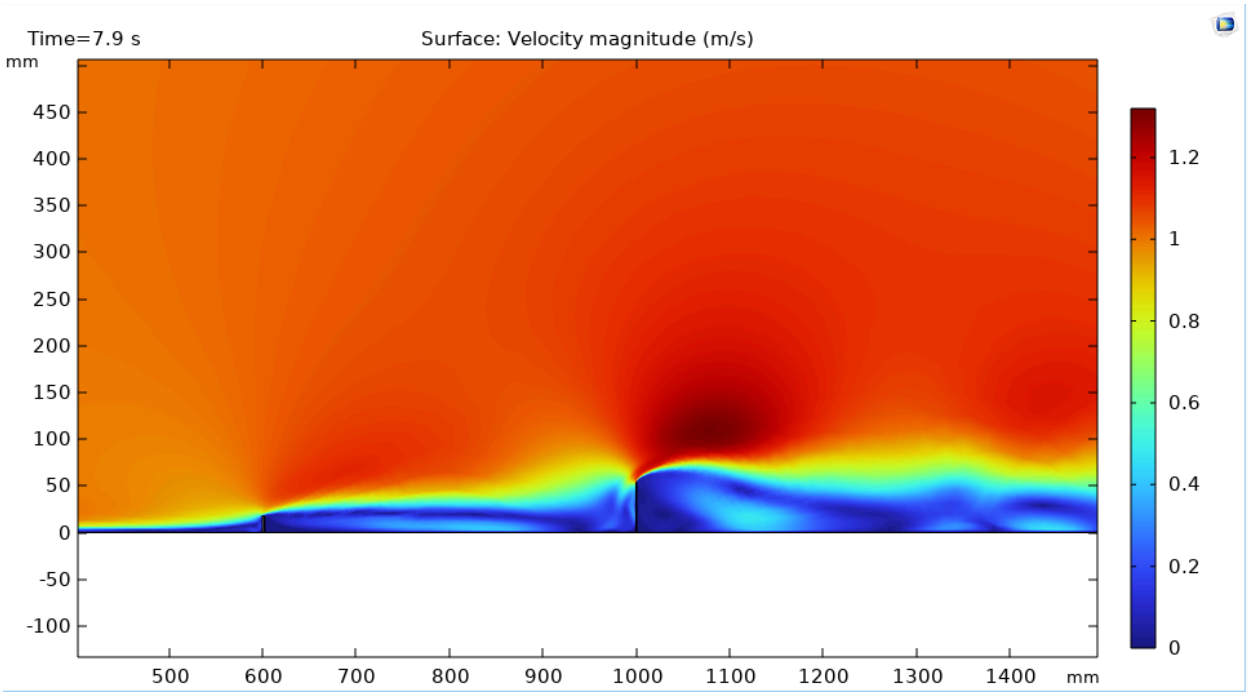

Figure 4.22 - Erratic oscillations velocity 7.9 seconds

The given time frame of 7.5-7.9 seconds shows a sharp increase in displacement of the piezoelectric beam which can be seen in Figure 4.5. In the pressure couture images (4.19-4.20), an area of low pressure followed immediately by an area of high pressure demonstrates the significant pressure change occurring on the front face of the piezoelectric beam. Likewise, in the velocity magnitude images (4.21-4.22), the section of high velocity can be seen crashing into the piezoelectric beam, generating the aforementioned deflection. While these deformations were significant, they were not as easy to predict as they did not follow an ideal sinusoidal curve and have a relatively large period.

Lastly, the predictable oscillatory behavior was observed when the size of the flow disruptor was relatively the same scale as the distance between it and the piezoelectric beam. This behavior tended to be less extreme than the erratic oscillatory behavior, yielding smaller amplitudes with smaller periods. The main difference between the two was that the predictable oscillatory behaviors were extremely predictable, and could be modeled as an exact sine curve in some cases. Figures 4.23 and 4.24 show the interaction of the pressure on the piezoelectric beam, while Figures 4.25 and 4.26 show the interaction of velocity on the piezoelectric beam over a 0.2-second period.

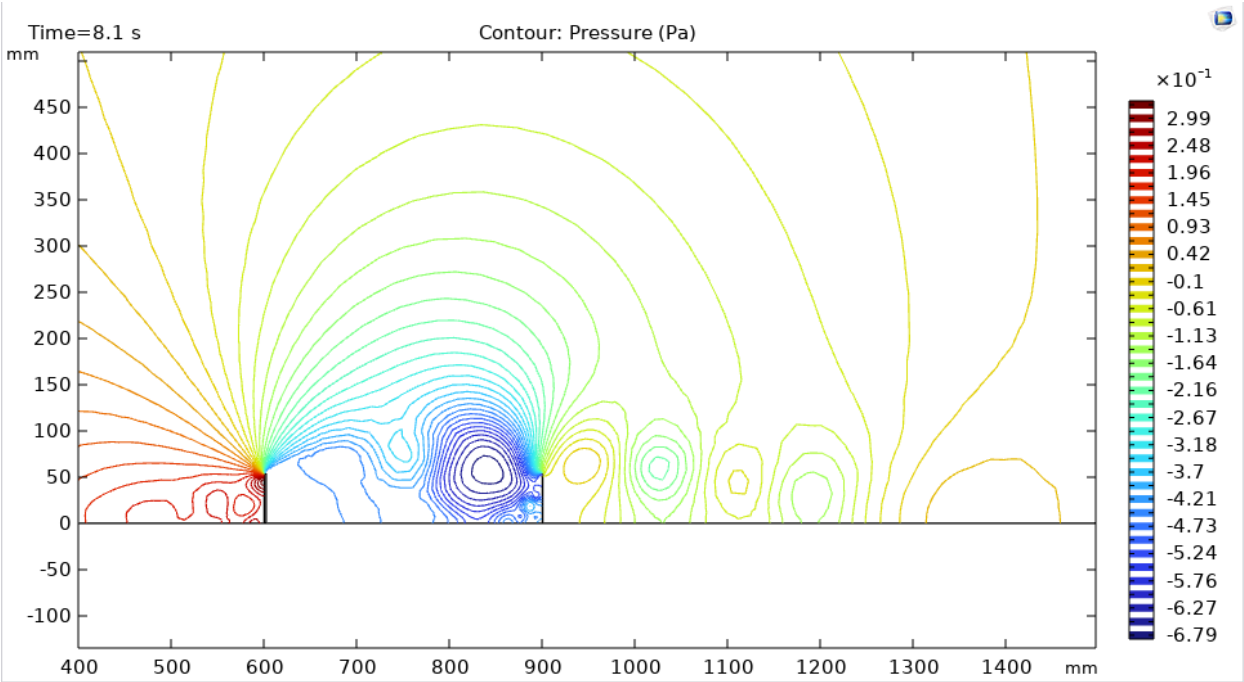

Figure 4.23 - Predictable oscillations pressure 8.1 seconds

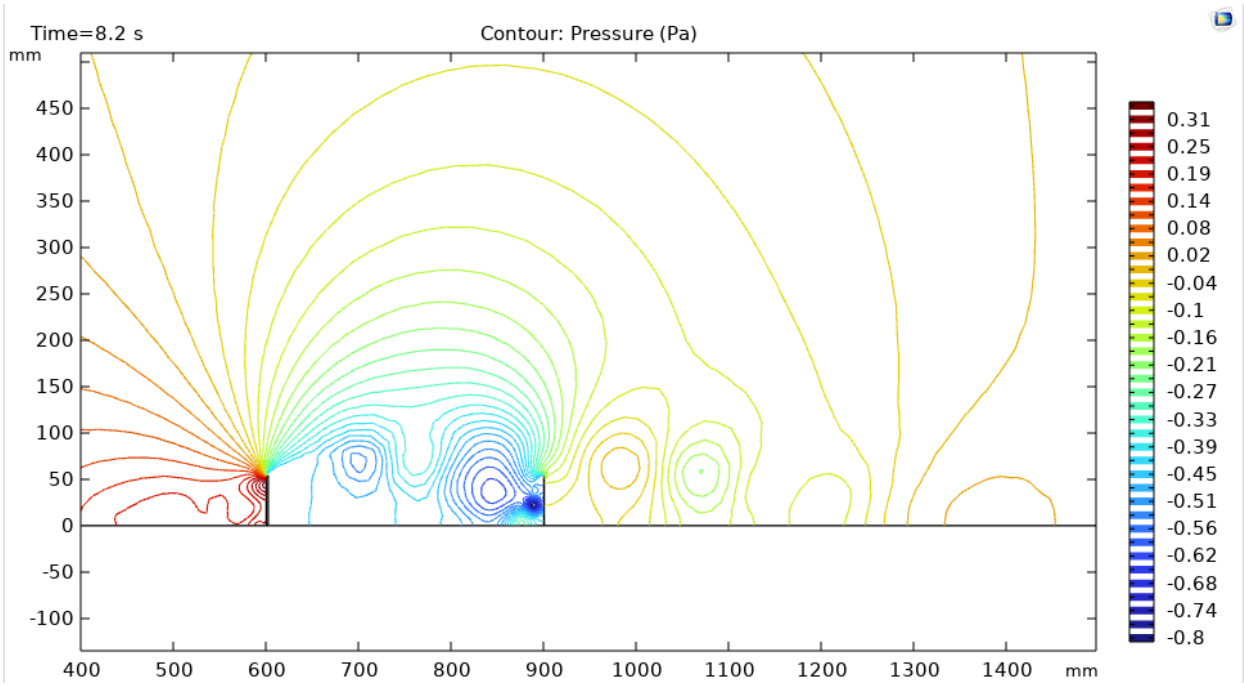

Figure 4.24 - Predictable oscillations pressure 8.2 seconds

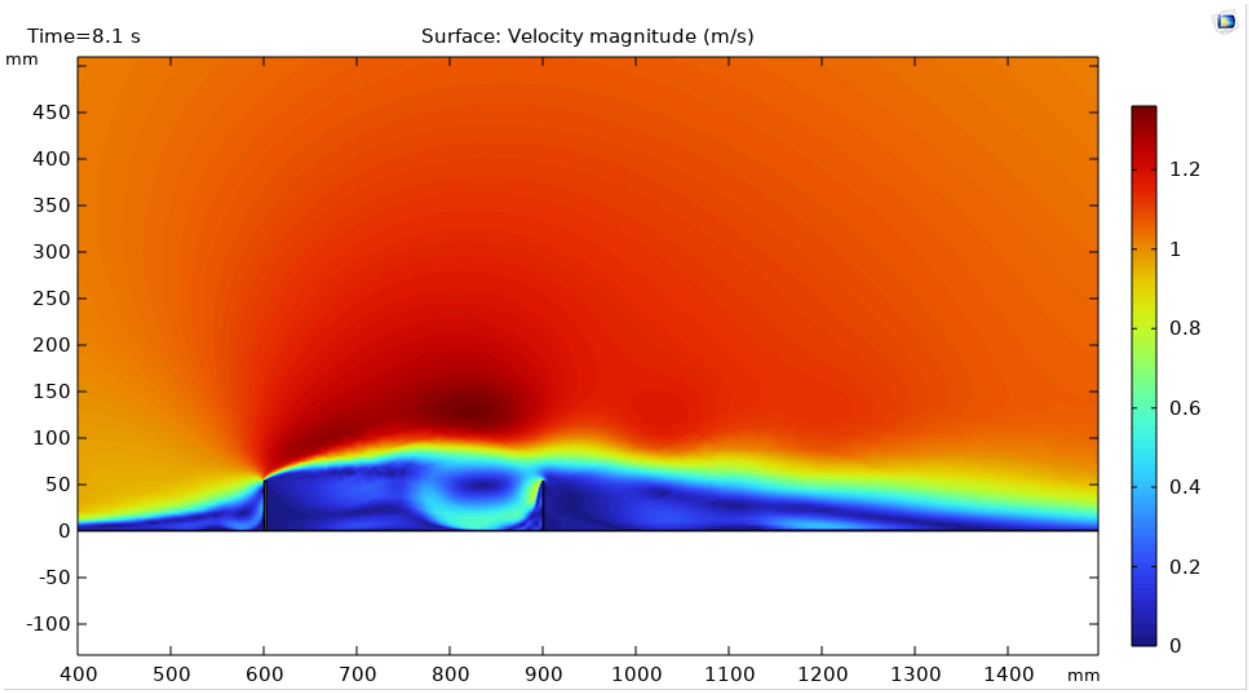

Figure 4.25 - Predictable oscillations velocity 8.1 seconds

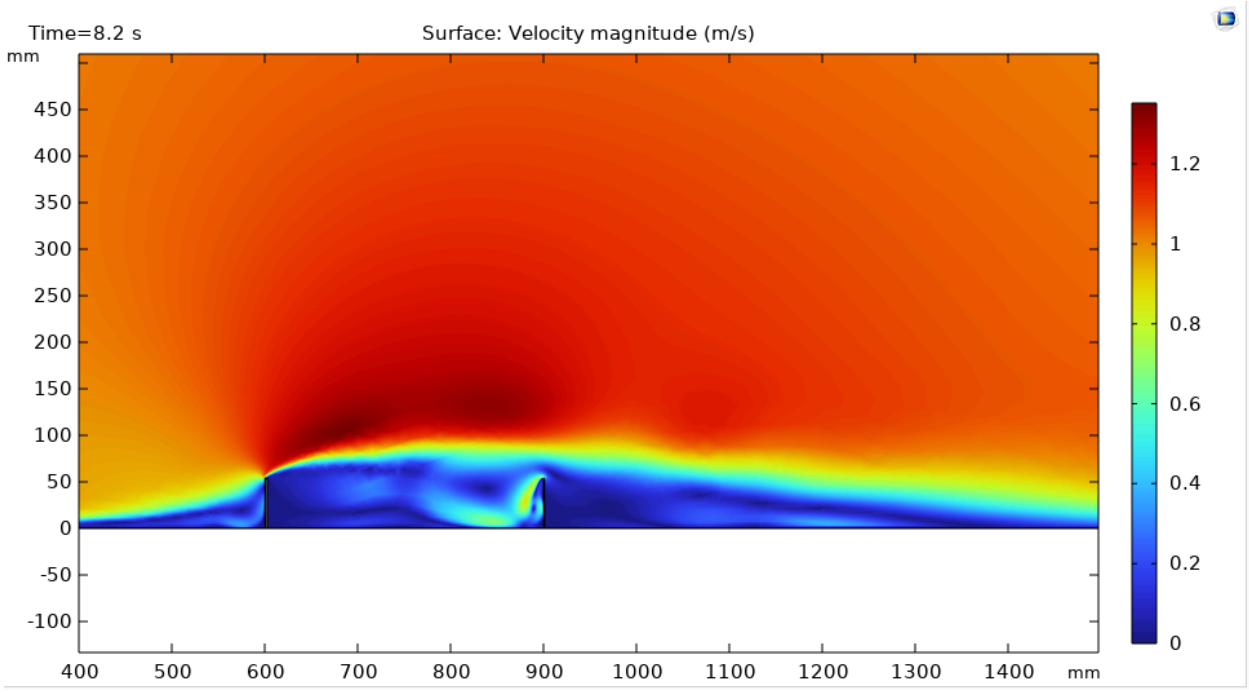

Figure 4.26 - Predictable oscillations velocity 8.2 seconds

In the above figures, the oscillation towards the right of the system was shown. For pressure (Figures 4.23-4.24) the area of low pressure moved around the area between the flow disruptor and piezoelectric beam, pushing and pulling the beam. In the velocity images (Figures 4.25-4.26), a strip of faster flow can be seen cresting over the top of the flow disruptor beam, pushing it gradually. The period of this system was approximately 0.4 seconds, which was much

faster compared to the erratic oscillation's period of approximately 1.5 seconds. The forces in the oscillatory systems was much more subtle, with minor changes in the pressure and velocity driving the high frequency oscillations. The subtle changes were difficult to capture through static images, however, a video provided a much more comprehensive representation.

4.2. Behavior of Beam Under Various Velocities

While the optimization of the geometry's configuration was essential for this study, observing the effects of different velocities was also important to understand how the geometries interact with each other. The predictable oscillatory behavior configuration was selected to observe the changing velocities as it had a very predictable pattern and the effect of the velocity could be easily quantified. Configuration 3 2, (Figure 4.2 and Figure 4.11) was used in this example. Figure 4.27 showed a comparison of inlet velocities of 0.9, 1.0, 1.1, 1.2, and 1.3 m/s, Figure 4.28 showed 1.3, 1.4, and 1.5 m/s, Figure 4.29 showed 1.5, 1.6, and 1.7 m/s, and Figure 4.30 showed 1.7, 1.8, 1.9, and 2.0 m/s

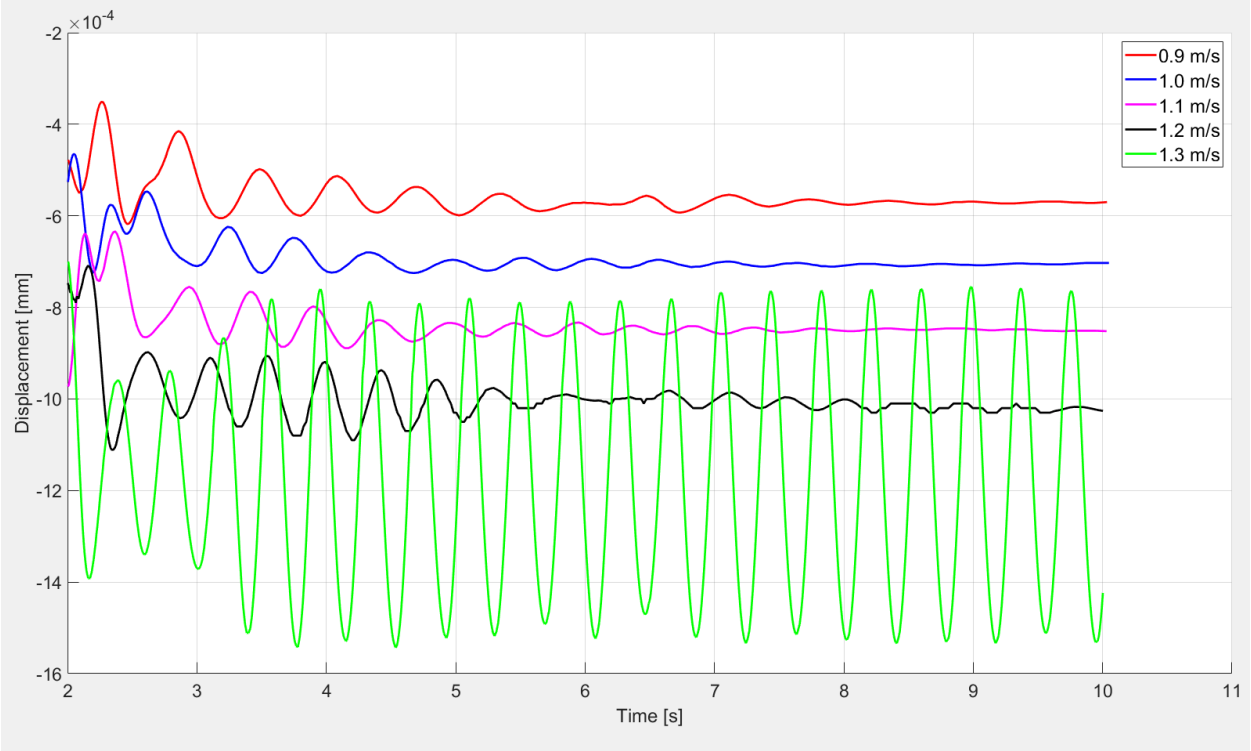

Figure 4.27 - Beam displacement 0.9-1.3 m/s

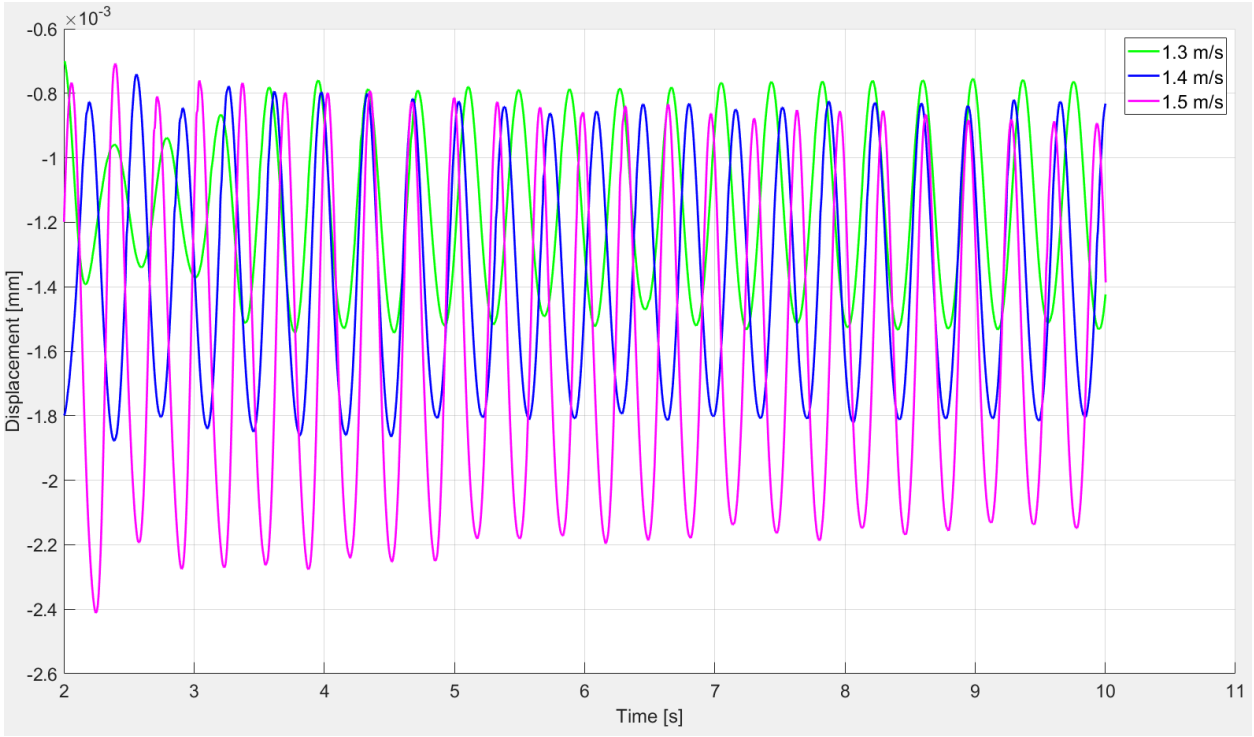

Figure 4.28 - Beam displacement 1.3-1.5 m/s

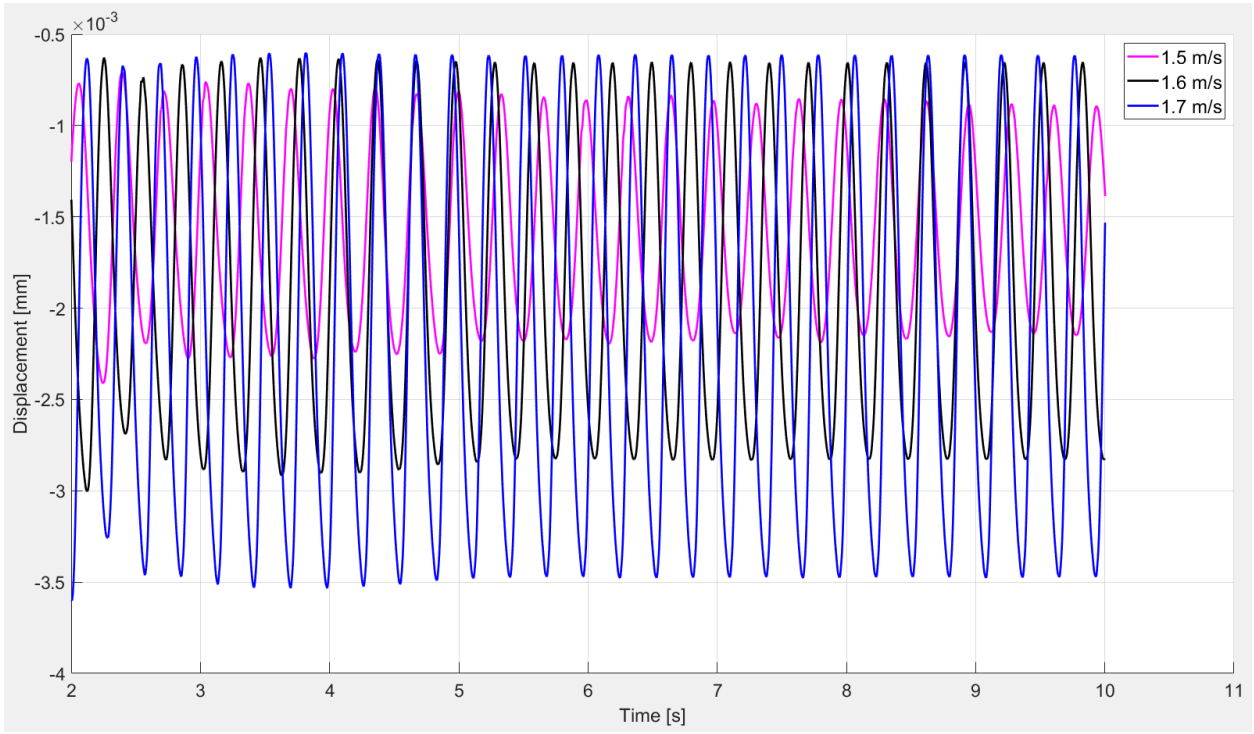

Figure 4.29 - Beam displacement 1.5-1.7 m/s

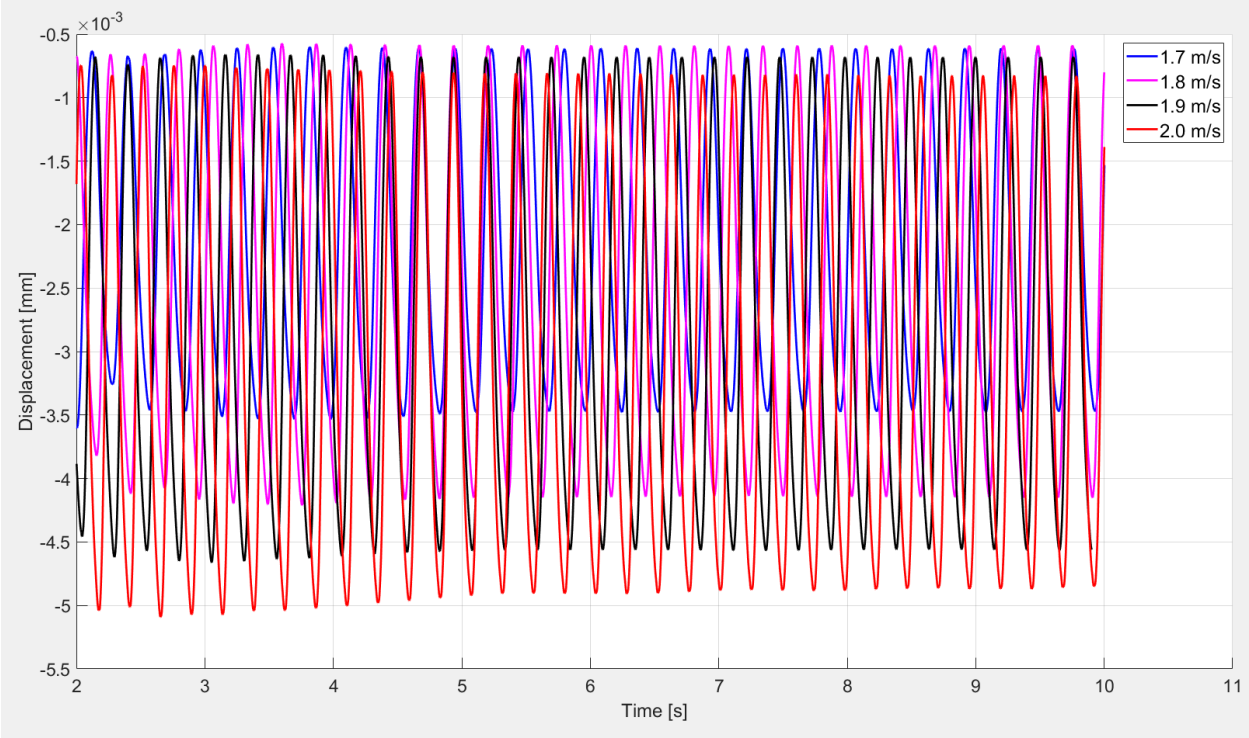

Figure 4.30 - Beam displacement 1.7-2.0 m/s

In all beam displacement graphs, the first two seconds were removed to look at data that had been stabilized. Figure 4.27 showed that at lower speeds, the beam was unable to maintain oscillations and eventually converged to zero for speeds of 0.9-1.2 m/s. Velocities of 1.3 m/s and higher were able to sustain stable oscillations. Figures 4.28-4.30 illustrated the displacement and frequency of oscillations increasing along with an increased velocity. When comparing 1.3 m/s to 2.0 m/s, the amplitude of oscillation increased by a factor of five. While this was not a sustainable trend, it indicated that the higher the inlet velocity, the larger the overall magnitude of displacement. Figure 4.31 showed velocities 1.5-2.0 m/s to illustrate the change of amplitude as the velocity increased. To avoid overcrowding the display, only the last second of the simulation was plotted. Figure 4.32 illustrates the relationship between inlet velocity and the average amplitude of the displacement.

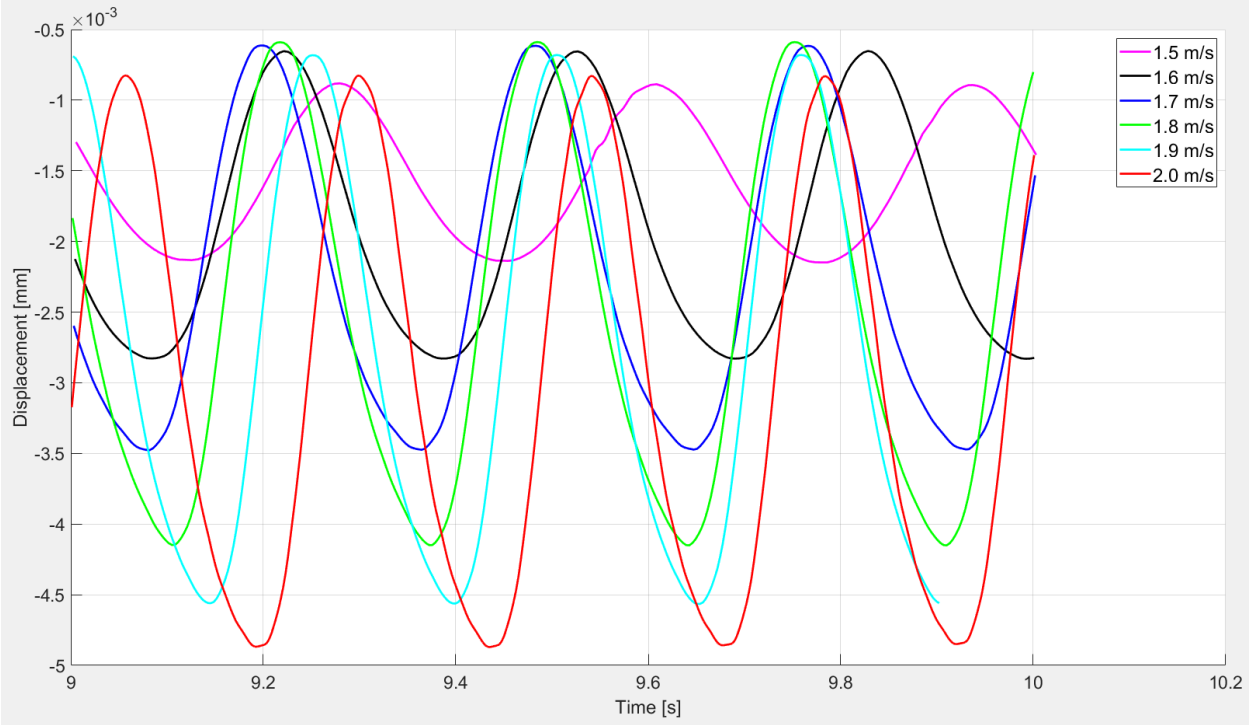

Figure 4.31 - Beam displacement 1.5-2.0 m/s, 9-10 seconds

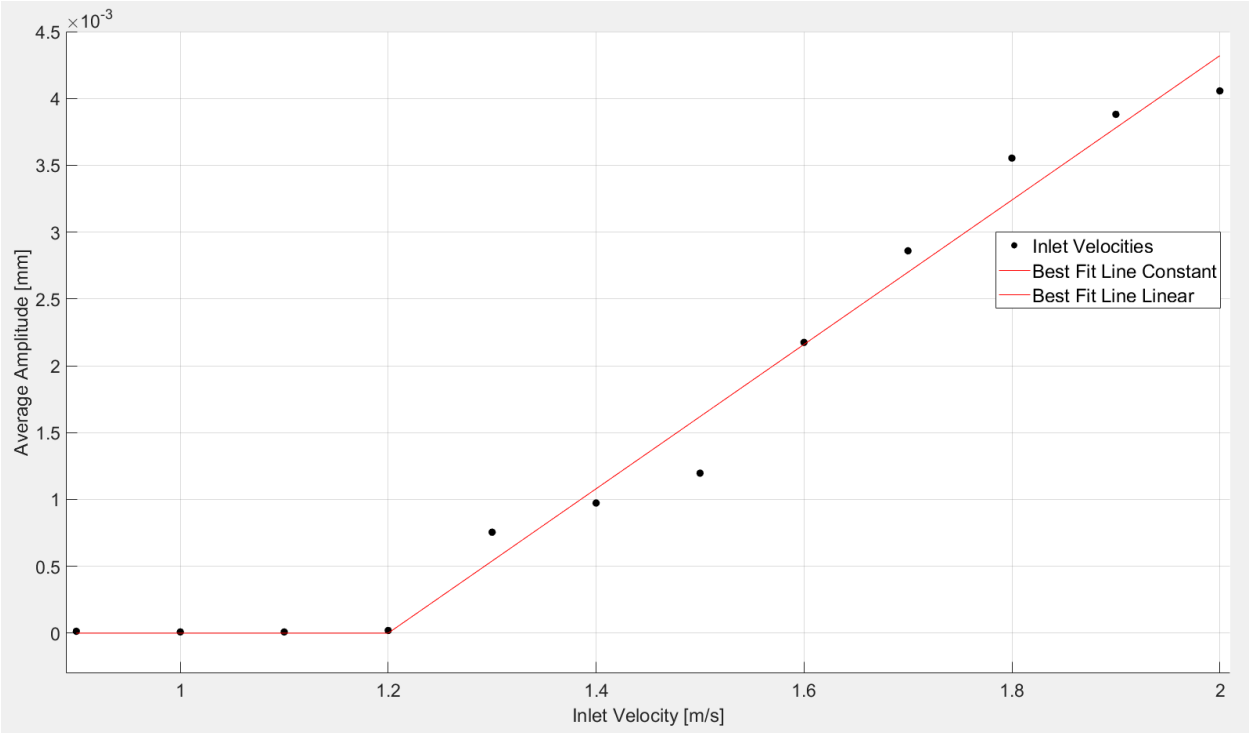

Figure 4.32 - Average amplitude vs. inlet velocity

It can be seen in Figure 4.32 that after 1.2 m/s, the magnitude of displacement begins to increase, so a linear line of fit best encompassed all data. Further velocities will need to be

investigated to verify these results. The results of these data are shown by Eq. (4.9). Assuming the trend continues, an increase in velocity will yield much higher displacements. A piecewise function was used to show that the results behave differently depending on the inlet velocity.

$$amp(v) = \begin{cases} 0 & 0 < v \leq 1.2 \\ 0.0054v - 0.00648 & 1.2 < v \end{cases} \tag{4.9}$$

Additionally, the relationship between the frequency of oscillations and the inlet velocity was studied. Due to the convergence to zero in the lower velocity, only the inlet velocities of 1.3-2.0 were shown in Figure 4.33.

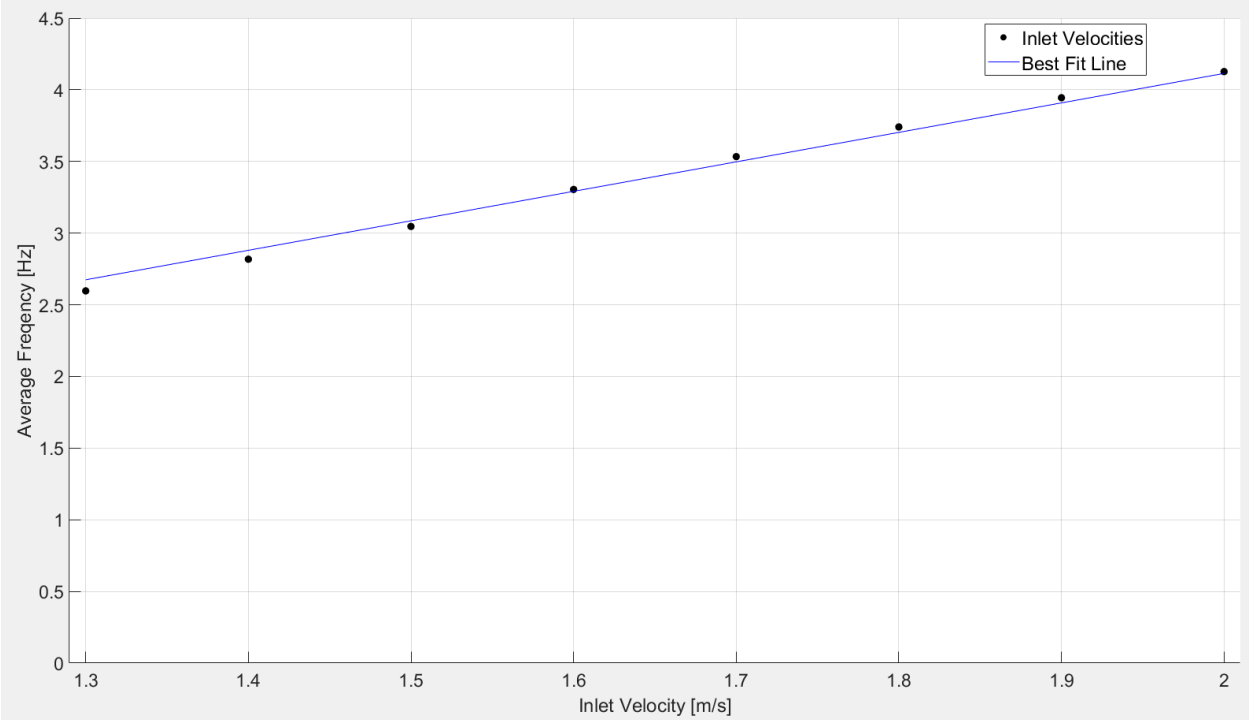

Figure 4.33 - Frequency vs. inlet velocity

There was a much more stable relationship between the frequency and velocity of the system, which can be partially explained by the removal of the lower inlet velocities. However, even when taking this into account, Figure 4.33 still illustrated that the relationship between frequency and velocity was more stable. This system followed a linear trend, implying a continuous frequency output of the system when increasing the velocity. Eq. (4.10) shows the formula of the line of best fit.

$$freq = 2.0571v \tag{4.10}$$

4.3 Energy Output

In the previous section, the predictable oscillation configuration was used to predictably track the frequency and amplitude of the displacement. However, a verification study was required to determine if another behaviour yielded a higher energy output. The other configuration to be considered was the erratic oscillations. In the predictable oscillation set up, a higher frequency was observed with lower displacement when compared to the erratic oscillations. Configurations 3 2 and 1 3 will be considered for this test.

Using an example of a piezoelectric energy harvester from the COMSOL Application Libary, the conditions from 3 2 and 1 3 were simulated, replicating both their frequency and displacement. Figures 4.34 and 4.35 show the beam displacement behavior, taken at 2 m/s, which was where the data was extracted from to determine the data points for the piezoelectric energy harvester simulation.

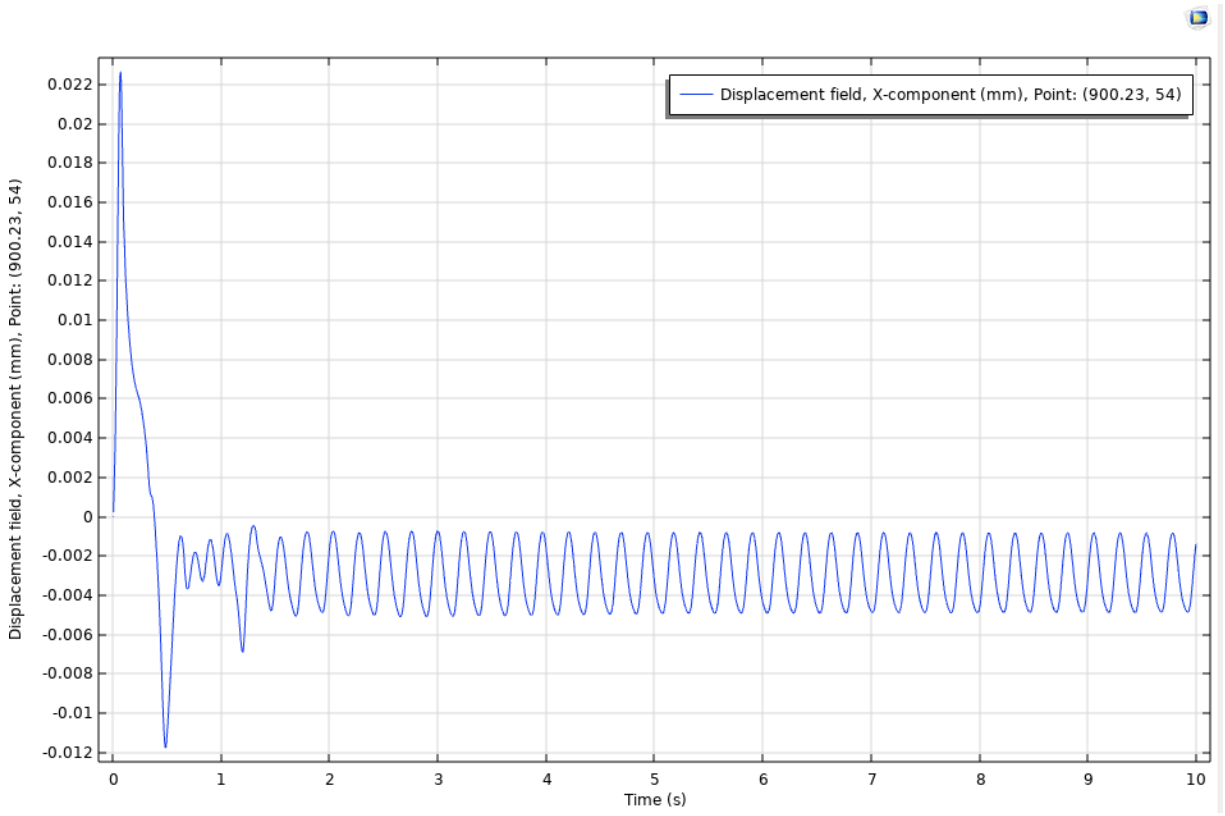

Figure 4.34 - Beam displacement 3 2

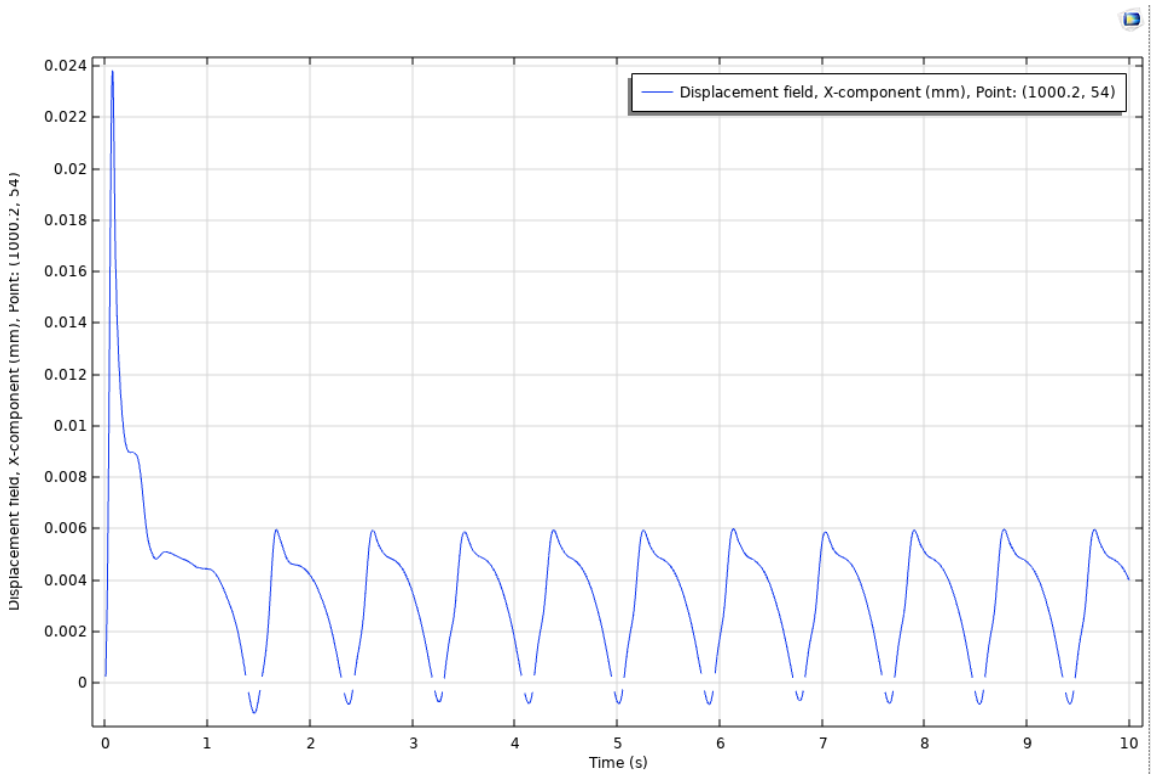

Figure 4.35 - Beam displacement 1 3

Figures 4.36 and 4.37 show the geometry and mesh of the energy harvester, which was modified to match the dimensions of the piezoelectric energy harvester used in the FSI simulation.

Figure 4.36 - Energy harvester geometry

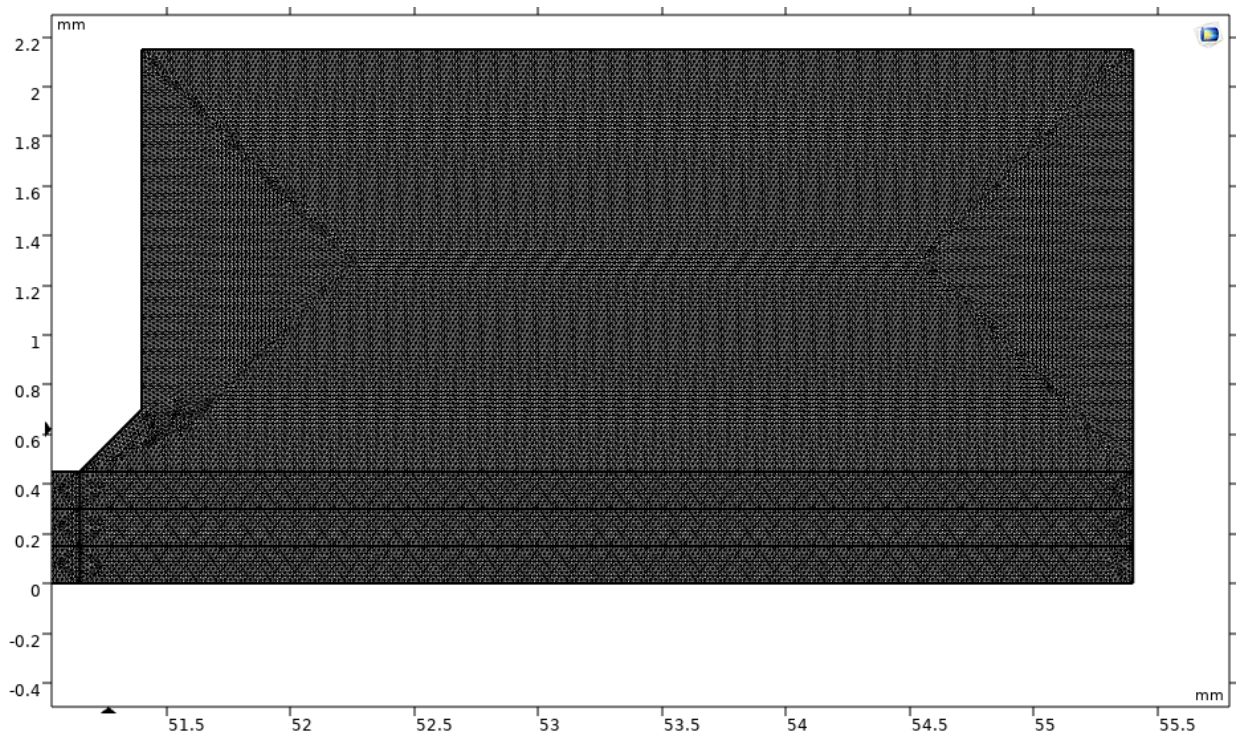

Figure 4.37 - Energy harvester mesh at tip

The voltage and power output were determined for both cases. Table 4.1 summarizes the results of the simulation for both configurations.

Table 4.1 - Energy harvester results for inlet speed of 2 m/s

Configuration	3 2: Predictable Oscillations	1 3: Erratic Oscillations
Frequency	4.125 Hz	1.133 Hz
Displacement	0.004056 mm	0.006766 mm
Voltage	0.0056 V	0.0025 V
Power	1.287×10^{-6} mW	2.698×10^{-7} mW

The first three rows summarized the initial values and conditions for the simulation. Rows four and five looked at the output of the simulation, with the power output being the most important variable. When looking at the predictable oscillations versus the erratic oscillations, the predictable oscillations yielded a power output one order of magnitude larger than erratic oscillations. This could be attributed to the higher frequency of the displacement, which coincided with the concept that higher frequencies tend to draw out more power from piezoelectric devices rather than larger displacements. While the device stayed well within the safe range, another factor to consider was that larger displacements run the risk of damaging the

device, so tending towards higher frequencies rather than larger displacements allowed for higher energy outputs and safer device operation.

Using the higher frequency configuration, the power output was explored at different velocities. As stated before, velocities of 0.9-1.2 m/s converged to zero once the simulation stabilized, so velocities of 1.3-2.0 m/s were studied in this section. The voltage produced could be seen in Figure 4.38, with a linear, upward trend in relation to the increased frequency and amplitude of the beam's displacement due to the increasing velocity.

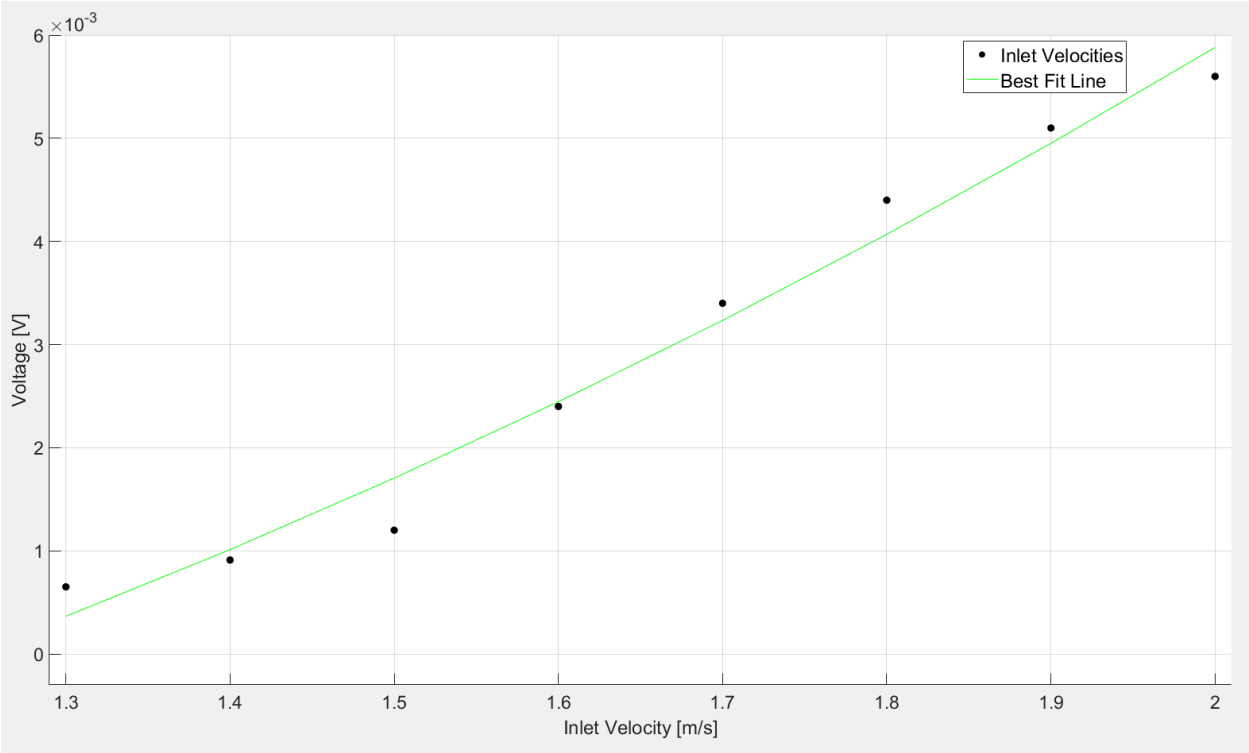

Figure 4.38 - Voltage vs. velocity

Aside from the voltage output doubling from 1.5 to 1.6 m/s, the output remained fairly constant, reaching a maximum value of 0.0056 volts at 2.0 m/s. The power output followed a linear shape, as seen in Figure 4.39, where the output had a linear trend after a relatively constant initial behavior.

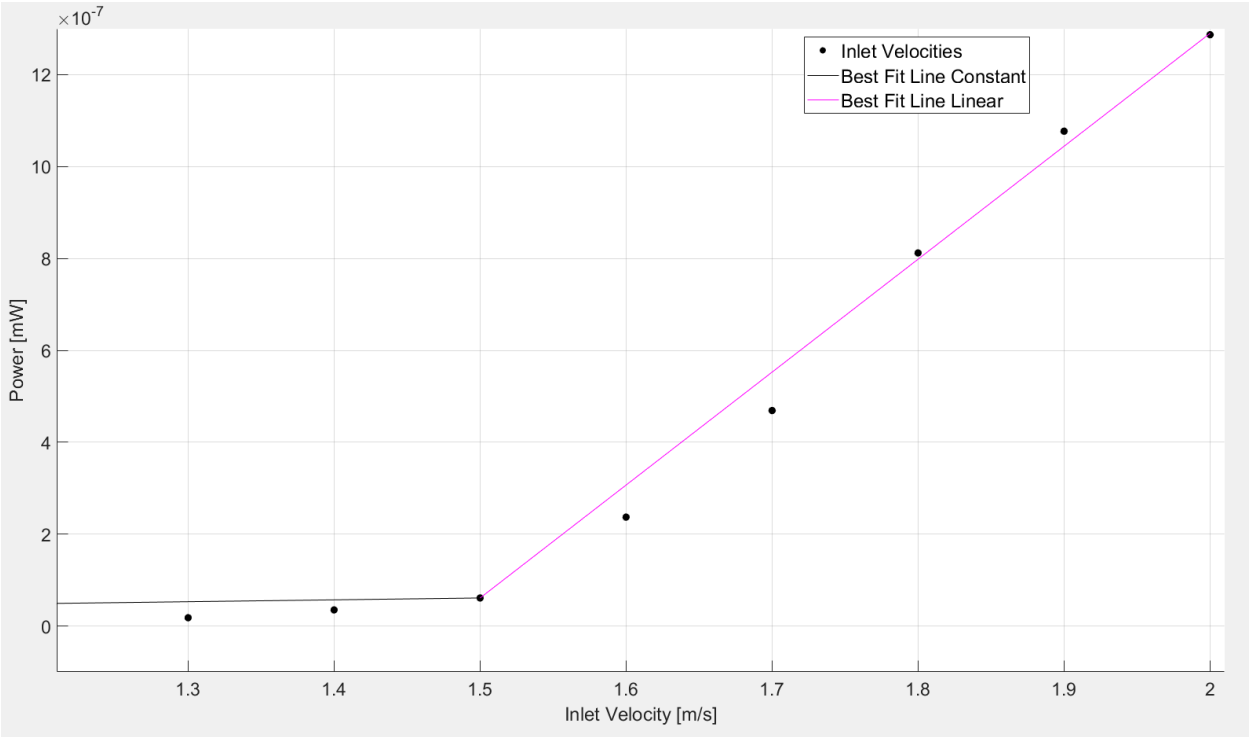

Figure 4.39 - Power vs. velocity

The power graph followed the linear piecewise equation as shown in Eq. (4.11)

$$power(v) = \begin{cases} 4.067 \cdot 10^{-8} v & 0 < v \leq 1.5 \\ 2.46 \cdot 10^{-6} v - 3.626 \cdot 10^{-6} & 1.5 < v \end{cases} \quad (4.11)$$

5. Discussion

The 30 simulations yielded four main outcomes: zero converging, erratic deflections, erratic oscillations, and predictable oscillations. Zero-converging results tended to occur when the turbulence-generating beam was either too large or too small and too close or too far from the piezoelectric beam. Erratic deflections occurred when the disruptor was large and too close to the piezoelectric beam. Erratic oscillations occurred when the disruptor was smaller and moderately close or far from the piezoelectric beam. Predictable oscillations occurred when the disruptor and piezoelectric beam were scaled proportionally with the distance between them and the size of the disruptor beam. These predictable oscillations yielded the highest power output, making them the ideal configurations. Beam displacement occurred when the turbulence generated from the flow disruptor interacted with the piezoelectric beam. Through more advanced turbulence models, higher speeds could be explored, potentially making more configurations viable or increasing power output of the existing predictable oscillation configurations.

The energy output of the deflecting piezoelectric beam was determined through a separate simulation of an individual deflecting piezoelectric beam undergoing the same conditions seen in its respective CFD simulation. Two separate cases were selected to determine the optimal beam behavior: higher frequency or higher displacement. The predictable oscillations were selected for higher frequencies (Fig. 4.34), and the erratic oscillations were selected for higher displacement (Fig. 4.35). When compared, the predictable oscillations yielded a higher voltage and power output, making it the ideal configuration for energy harvesting, in addition to long-term reliability. If the larger deflections yielded more power, then a separate analysis would have to be performed to determine if the extra power would be worth the potential damage to the beam. Based on these results, more simulations were performed on the cases that yielded stable predictable oscillations. These simulations showed that the voltage and power output increased at a linear rate after a certain velocity threshold was passed. Since these simulations looked at a relatively small velocity sample, further simulations would have to be run to determine where the energy output decreases, as it is unrealistic to assume that the power output continues at a linear rate.

When compared to existing literature, few studies have studied energy harvesting with a fluid disruption system. Lee et al. [21] is one study that simulated a similar geometry as shown in this report, and how various geometry configurations impacted power output. Their study simulated multiple beams and how the power output varied in different formations. The various formations produced 0.8-1.6 nW of power, compared to the 1.2 nW of power produced in the results specified above. However, further simulations will need to be run for a definitive comparison, as this project only simulated a single beam while Lee et al. simulated an array, which could lead to inaccurate assumptions.

The biggest limitation of this study was the inability to use a turbulence-based model. To accommodate this, lower inlet speeds were used to prevent the Reynolds number from getting far into the turbulent regime. Ideally, speeds up to 10 m/s would have been tested, but the speeds ran in the simulations provide an acceptable amount of information to establish a baseline for power and general turbulence output.

The next step of this study would be to explore how the energy harvesting beams behave in a series of harvesters. In practical applications, there would not be a stand-alone harvester, but multiple harvesters in configuration. These harvesters would generate turbulence for the downstream harvesters, leading to flow disruptors either only at the beginning of the flow or

occasionally dispersed throughout the system. Finally, a 3D model of the aforementioned series of harvesters would be simulated to determine the behavoir in practical applications.

6. Conclusion

Renewable energy sources continue to be a desirable alternative to fossil fuels in every sector around the world. One application of renewable energy would be a replacement for batteries, which require maintenance whenever they run out of charge. In smaller cases, piezoelectric energy harvesters may be a viable alternative. For systems in a fluid flow, either air or water, utilizing artificially generated turbulence to vibrate a piezoelectric beam acts as a potential alternative for batteries in systems that are difficult to provide maintenance to. The results of this study indicate that it would be possible to harvest energy in certain geometric configurations. Using a thin cantilever beam positioned upstream from the piezoelectric beam, multiple configurations were tested, exploring both spacing between the beams and the size of the flow disrupting beam. These configurations resulted in one of four possible behaviors: the oscillations of the beam converging to zero, erratic deflection behavior, erratic oscillations, or predictable oscillations. An analysis of the power output of the erratic oscillations and predictable oscillations was performed to determine that predictable oscillations produced a higher energy output, likely due to the higher frequency of displacement. Various velocities were also explored and its influence on the displacement of the beam and on the energy output were discussed. There was a clear relationship between increased velocity and energy output of the oscillating piezoelectric beam. Future studies should look at how energy output is related to a series of energy harvesters, both in 2D and 3D simulations. This was the biggest limitation of this study, as turbulent flow was not supported in the COMSOL FSI academic license. Further studies should also look at how a higher range of velocities (5-10 m/s) would impact the energy harvesters and how much more energy would be produced in a variety of geometrical configurations.

References

[1] Staff, E, “U.S. energy consumption increases between 0% and 15% by 2050”, *U.S. Energy Information Administration (EIA)*, 3 April 2023. Retrieved 30 September 2024 from <https://www.eia.gov/todayinenergy/detail.php?id=56040>

[2] Lakeh, H, “What are the Pros and Cons of Renewable Energy?”, *GreenMatch*, 27 March 2024. Retrieved 30 September 2024 from <https://www.greenmatch.co.uk/blog/2021/09/advantages-and-disadvantages-of-renewable-energy>

[3] Sekhar, B. C., Dhanalakshmi, B., Rao, B. S., Ramesh, S., Prasad, K. V., Rao, R. S., and Rao, B. P., “Piezoelectricity and Its Applications,” *Multifunctional Ferroelectric Materials*, IntechOpen, 2021, pp. 71-88.

[4] Uchino, K., “The development of piezoelectric materials and the new perspective,” *Advanced Piezoelectric Materials*, Woodhead Publishing Limited, 2010, pp. 1-21

[5] “The History of Piezoelectricity”, *OnScale*, (n.d.). Retrieved 30 September 2024 from <https://onscale.com/piezoelectricity/history-of-piezoelectricity/>

[6] Dong, H., Zhu, Z., Li, Z., Li, M., and Chen, J., “Piezoelectric Composites: State-of-the-Art and Future Prospects,” *The Journal of The Minerals, Metals & Materials Society*, Vol. 76, No. 1, 2023, pp. 340–352.

[7] Sekhar, M. C., Veena, E., Kumar, N. S., Naidu, K. B., Mallikarjuna, A., and Basha, D. B., “A Review on Piezoelectric Materials and Their Applications,” *Crystal Research and Technology*, Vol. 58, No. 2, 2022.

[8] “Material Properties”, *Piezo Support*, 16 November 2020. Retrieved 30 September 2024 from <https://support.piezo.com/article/62-material-properties>

[9] Saito, Y., Takao, H., Tani, T. et al., “Lead-free piezoceramics,” *Nature*, Vol. 432, No. 7013, 2004, pp. 84–87.

[10] Savin, V. V., Keruchenko, M. A., Ershov, P. A., Vorontsov, P. A., Ignatov, A. A., and Rodionova, V. V., “Studying Physical Properties of a Polyvinylidene Fluoride/Lead Zirconate Titanate Piezoelectric Composite,” *Bulletin of the Russian Academy of Sciences: Physics*, Vol. 88, No. 4, 2024, pp. 577–581.

[11] Bowen, C. R., Kim, H. A., Weaver, P. M., and Dunn, S., “Piezoelectric and ferroelectric materials and structures for energy harvesting applications,” *Energy & Environmental Science*, Vol. 7, No. 1, 2014, pp. 25–44.

[12] Mallouli, M., Chouchane, M., “Fiber Material and Electrode Configuration Selection in Designing Piezoelectric Macro Fiber Composites,” *Design and Modeling of Mechanical Systems*, *CMSM 2023*, Switzerland, August 2024.

[13] Covaci, C. and Gontean, A., “Piezoelectric Energy Harvesting Solutions: A Review,” *Sensors*, Vol. 20, No. 12, 2020.

[14] Chen, X., Yang, T., Wang, W., and Yao, X., “Vibration energy harvesting with a clamped piezoelectric circular diaphragm,” *Ceramics International*, Vol. 38, 2012, pp. 271–274.

[15] Palosaari, J., Leinonen, M., Hannu, J., Juuti, J., and Jantunen, H., “Energy harvesting with a cymbal type piezoelectric transducer from low frequency compression,” *Journal of Electroceramics*, Vol. 28, No. 4, 2012, pp. 214–219.

[16] Heller, L. F., Brito, L. A. T., Coelho, M. A. J., Brusamarello, V., and Nuñez, W. P., “Development of a Pavement-Embedded Piezoelectric Harvester in a Real Traffic Environment,” *Sensors*, Vol. 23, No. 9, 2023.

[17] Tuma, C. and Phaoharuhansa, D., “Vibration Energy Harvest for Low Frequency using Double-piezoelectric Cantilever Beam,” *MATEC Web of Conferences*, *ICMME 2019*, Osaka, Japan, 2020.
[18] Yayla, S., Ayça, S., and Oruç, M., “A case study on piezoelectric energy harvesting with using vortex generator plate modeling for fluids,” *Renewable Energy*, Vol. 157, 2020, pp. 1243–1253.
[19] An, X., Song, B., Tian, W., and Ma, C., “Design and CFD Simulations of a Vortex-Induced Piezoelectric Energy Converter (VIPEC) for Underwater Environment,” *Energies*, Vol. 11, No. 2, 2018.
[20] Zhao, L., Yang, Y., “On the modeling methods of small-scale piezoelectric wind energy harvesting,” *Techno-Press*, Vol. 19, No. 1, 2017, pp. 67-90.
[21] Lee, Y. J., Qi, Y., Zhou, G., and Lua, K. B., “Vortex-induced vibration wind energy harvesting by piezoelectric MEMS device in formation,” *Scientific Reports*, Vol. 9, No. 1, 2019.